الجمهورية الجزائرية الديمقراطية الشعبية
People's Democratic Republic of Algeria
وزارة التعليم العالي و البحث العلمي
Ministry of Higher Education and Scientific Research

المدرسة الوطنية العليا للتكنولوجيا و الهندسة - عنابة
National Higher School of Technology and Engineering – Annaba

Department of Process Engineering and Energetics

In Partial Fulfillment of the Requirements

for the
MASTER DEGREE

Field of Study: Energy

Presented by

AMIRAT Hakim

CFD Analysis and optimization of an Axial Flow Turbine

Supervised by

Associate Professor. BELAMADI Riyadh
NHSTE Annaba

Examination Board :

- Associate Professor. NIOU Akrem Slimane — President – NHSTE Annaba
- Associate Professor. KAHALERAS Mohamed Saïd — Examiner – NHSTE Annaba

Academic Year 2025

Remerciements

Ce travail est le fruit de trois années de formations en cycle ingénieur, durant toute cette durée, un bon nombre de personnes ont participé, directement ou indirectement à atteindre ce stade et pouvoir réaliser ce travail.

Tout d'abord, je souhaite adresser mes vifs remeciements à mon encadrant Riyadh BELAMADI pour sa précieuse aide tout au long de cette période, pour ses conseils et sa rigueur, ses encouragements m'ont motivé à toujours donner le meilleur de moi-même, ce qui a fait de ce travail ce qu'il est aujourd'hui.

Je souhaite également remercier Mohamed Saïd KAHALERAS, pour les longues discussions que l'on a eu et ses conseils qui m'ont aidé à avancer.

Pour finir, je souhaite témoigner ma profonde gratitude à tous les enseignants chez qui j'ai eu cours, de tous départements confondus, ainsi que tout le personnel de l'école qui ont rendu l'environnement de travail agréable et jovial, j'en garderai de précieux souvenirs.

À mes parents, et à ma tante Zaïna.

Résumé

Ce travail a présenté l'approche utilisée pour simuler une turbine conçue grâce à un algorithme écrit en code puis en utilisant la CFD pour l'étude des performances de la machine. Le package ANSYS CFX (TurboGrid, Pre, CFX, Solver Manager et CFD-Post) a produit des résultats précis et fiables en utilisant un modèle robuste de turbulence K ω SST pour l'écoulement stationnaire. Les résultats obtenus étaient proches des points de conception, avec quelques différences dues aux simplifications préliminaires. La simulation nous a permis de créer une carte des performances du premier étage de la turbine. Enfin, une simulation complète de la turbine conçue a été réalisée pour avoir une vue d'ensemble opérant dans des modèles mathématiques à haute fidélité.

ملخص:

قدّم هذا العمل المنهج المُستخدم لمحاكاة توربين مُصمّم باستخدام خوارزمية مُرمّزة، ثمّ ديناميكيات الموائع الحسابية (CFD) لدراسة أداء الآلة .أنتجت حزمة ANSYS CFX (TurboGrid، Pre، CFX، Solver Manager، وCFD-Post) للتدفق الثابت .كانت النتائج المُتحصّل عليها Kφ SST نتائج دقيقة وموثوقة باستخدام نموذج اضطراب قوي لـ قريبة من نقاط التصميم، مع بعض الاختلافات الناتجة عن التبسيطات الأولية .أتاحت لنا المحاكاة إنشاء خريطة أداء للمرحلة الأولى من التوربين .وأخيرًا، أُجريت محاكاة كاملة للتوربين المُصمّم للحصول على نظرة عامة على العمل في نماذج رياضية عالية الدقة.

Abstract

This work has presented the approach used to simulate a designed turbine through an algorithm we implemented in a code, then using CFD to investigate the performance of the machine. The CFD method by using the ANSYS CFX tool (TurboGrid, Pre, CFX, Solver Manager and CFD-Post) showed accurate and solid results by using a robust turbulence model K ω SST for the steady flow, The results found were close to the design points with some differences due to the preliminary simplifications. The simulation allowed us to create a performance MAP for one stage turbine design, in the end a simulation of the whole full configuration turbine design was made to have an overview of the complete machine in high-fidelity models.

Keywords: Computational Fluid Dynamics, Turbomachinery, Axial Flow Turbine, Axial Rotor.

Nomenclature

Nomenclature

ω Rotational Speed

P_{t_i} Total Pressure at i station

T_{t_i} Total Temperature at i station

$\dot{m}$ Mass Flow Rate

θ Divergence Angle

η_{t-t} Total-to-total efficiency

h Entalphy

α_i Absolute Flow Angles

N_s Specific Speed

C_p Heat Capacity

r_m Mean Radius

ρ Static Density

Δh_{id} Ideal Work

Pr Total Pressure Ratio

V_0 Inlet Velocity

V_z Axial Velocity

β Relative Flow Angle

ϕ Flow Coefficient

ψ Work Coefficient

R Stage Reaction

W Relative Speed

T_{t_r} Total Relative Temperature

M Mach Number

M_r Relative Mach Number

$M_{r_{cr}}$ Critical Relative Mach Number

U_m Maximum speed at mean radius

U Peripheral Speed

R Universal Gas Constant

V Absolute Velocity

λ Axial Aspect Ratio

h Height

C_z Axial Chord

ΔZ Axial Gap

xi Deflection Angle

s Pitch

(s/c) Pitch-to-Chord Ratio

F_{AR} Sheet Area Ratio

c Blade Chord

β_g Gauge Angle

N Number of Blades

AR Axial Aspect Ratio

List of Figures

List of Tables

Contents

Introduction

The continuous aim to a maximized efficiency and performances of energy production systems has led power plant and aerospace engineers to implement new ways of optimisation of turbomachinery components in their field working engines. For propulsion systems, the axial flow turbine plays an important role in extracting the fluid's energy particularly when it comes to turboprop engines to ensure the necessary thrust to drive the aircraft, as the performance of the turbines is crucial for the efficieny of an aircraft. Therefore, all improvements regarding the aerodynamic or thermodynamic aspect of the turbine designs can lead to a lower fuel consumption, higher thrust outputs and greater designs operational ranges.

Nowadays, since the axial turbine is the component that extracts the mechanical energy from high-pressure and temperature conditions in the combustion chamber's exit to correctly drive the propeller, therefore, the design of the axial turbine should reach a good balance between manufacturability, aerodynamic efficiency and also manufacturability. By having a strong focus on the lowering the fuel consumptions (and gas emissions, for environment causes). Designers must then offer configurations that carries minimal losses, lightweight compact, and durable under challenging (often extreme) flying conditions (Ex: Turbulence).

To meet the commercial and military expectations. Designers has evolved by including several modeling approaches of axial tubines. The well-known meanline design remains a great contender to any new design thus allowing a fast estimation of key parameters as such as number of stages, velocities, Mach Number (to ensure being in the correct flow domain ie. subsonic, supersonic), blade profiles and thermodynamic performance according to the limitations imposed by the client, all these parameters influence directly the behaviour of any turbine configuration.

With the growing mathematical coupled to physical knowledge of the modern times, strong numerical schemes and methods often called Computational Fluid Dynamics (CFD) has become an integrated tool in the design analysis of turbomachinery components thus axial turbines. While empirical correlations and mean-line approaches offer a strong theoretical design and provides valuable insights in the preliminary stage design, they often lack the fidelity required to fully capture the 3-D flow behaviour occuring within the blade passages, thus engineers can visualise flow separations, shock waves and secondary flows if necessary. They can have a deeper understanding of how their configuration operates in close-to-real conditions. Therefore CFD has been implemented as an important part of any turbomachinery design as optimisation and even parametrical studies are met to explore the depth of the working range of any machine.

Chapter 1

Background and motivation

In a previous academic project, a complete design for an axial flow turbine of a turboprop was made. It involved the preliminary design of aerodynamic parameters and geometric construction by a mean-line approach, aswell as a blade construction for all stators and rotors. The design methodology included optimizing the number of stages by respecting the working range of axial configurations since for propulsion systems, designers avoid radial configuration due to their less appropriate compactness [1] which leads us to effectively divide the workshaft among the stages (if more than one) regarding the restirctions and limitations. The velocity triangles are then calculated and optimised in a way to reach a typical axial stage (50 % of reaction), calculating the thermodynamic dimensions, geometric dimensions and finally, the blade profiles in respect to the design flows. a code was developed to automate the entire design, making the design become an optimisation problem, which is a good approach as it allows the designer to have a better view or pathwork for any given input and output parameters. [2] The code also provides the 2D Sketch of the airfoils.

The current work aims to expand this work by carrying out numerical simulations of the designed axial turbine which includes conducting calculations to estimate the design-point parameters to have a better view on the machine in working conditions. Turbulence modeling will be used to capture the flow characteristics in sensitive cases. The goal of this work is not only to estimate the performance of the turbine in nominal conditions but also to explore it's range of working conditions.

Our study will investigate the influence of some key parameters, such as aspect ratios, for which will be changed by using correlations for stator and rotors axial lengths, a study is also driven regarding inflow angle, therefore to have a better view for the combustion chamber's outlet possible allowable angles helping it's designer to know his components limitations. A work will also be done regarding the turbine performance over a range of pressure and rotational speeds to get enough data to draw the turbine map.

By combining the two phase of work being the preliminary theoretical design and the numerical modeling and simulation, we aim to contribute to a better understanding of our turbine design and it's optimal working conditions, and may it serve to future works for the complete design of a turboprop engine.

Chapter 2

State of Art

The computational Fluid Dynamics method became a widely used method to solve high-complexity equation for fluids, with its numerical implementations and high-level solvers such as Ansys FLUENT Solver, OpenFOAM opensource's code and many more, CFD became a serious and relevant tool in the scientific community, in this regard, there are some of the previous works concerning axial tubines

Hosseini and Al

Hosseini and Jafaripanah (2024) [3] performed a Computational Fluid Dynamic study with a genetic optimisation algorithm for a two-stage high pressure axial turbine where they investigated and improved some parameters such as polytropic efficiency and power, demonstrating that the adjusting geoemtrical parameters (such as stagger angle) can have a significant positive effect on the machine.

Vinícius Guimarães Monteiro and al

Vinícius Guimarães Monteiro and al [4] and al conducted a study following the RANS-Based Spalart-Allmaras turbulence model in several on and off design conditions of a first-stage axial turbine, the results of the numerical simulation were validated against a 1D model enhancing the efficiency of the CFD method.

Elqussas and al

Elqussas et al. [5] used a surrogate-based optimisation strategy by computing more than 120 numerical simulations on ANSYS CFX tool to improve a stage efficiency by controlling mass flow and pressure distributions through the blade shape thickness distributions.

Abdulhasieb and al.

Abdulhasieb et al. (2025) [6] worked on a CFD-based optimisation of an axial impulse turbine for tidal energy conversion, aiming to improve the overall efficiency by manipulating the rotor's inlet and outlet angles by a response surface applied methodology.

With all these works (and many others) we can assume the importance of the implementation of computational fluid dynamics in the design of any, let's say, industrial equipment. Therefore, our study will revolve around CFD.

Chapter 3

CFD Implementation

3.1 Design of the turbine

The designed turbine axial is composed by three stages, each carrying one stator and rotor cascade row. The multistage configuration is often adopted for turboprop engines as it allows the optimal work of axial stages with the needed amount split where stages are necessary to extract the energy from the high temperature and pressure exiting the gas chamber. In order to simplify the numerical analysis and reduce computation time, we investigate the numerical simulation on a single representative stage (Entry of the turbine, first stator, and exit of the stage, first rotor). This approach can give us a good approximation of the turbine design by estimating one stage. This approach creates a good balance between model fidelity and computational efficiency. Later, simulation will be performed for the whole turbine. The first stator is constituted by 49 blades, and the first rotor is constituted by 45 blades. the number of blades was calculated by R. Aungier correlations by respect to key parameters such as stagger angles, optimal pitch-to-chord, gauge angles..etc. The aspect ratio was taken to be taken gradually increasing for a first configuration before investigating its effect on the turbine performance later-on

Table 3.1: Axial Lengths

Stage	Component	Axial Length $[mm]$
1	Gap Inlet	3.526
	Stator	13.283
	Interstage Gap	7.05
	Rotor	14.98
	Gap Outlet	8.761

An important parameter here is the gaps, when defining the key parameters to meridional flow path and points where to inerpolate the blade heights. They are taken, in the inlet before the stator, and in the middle of the turbine its taken in the middle between one component and the other. These gaps are defined as follow:

$$\Delta Z_{stator-rotor} = \frac{h_{stator_i} + h_{rotor_i}}{4} \tag{3.1}$$

$$\Delta Z_{inter\ stage} = \frac{h_{stator_i} + h_{rotor_{i+1}}}{2} \tag{3.2}$$

With the gaps and axial length known, we must find the blade coordinates for the given component, our code provides the 2D Sketch and saves the coordinates, which is important for later CAD generation. Here below is the figure for both stator and rotor 2D Sketch Profiles

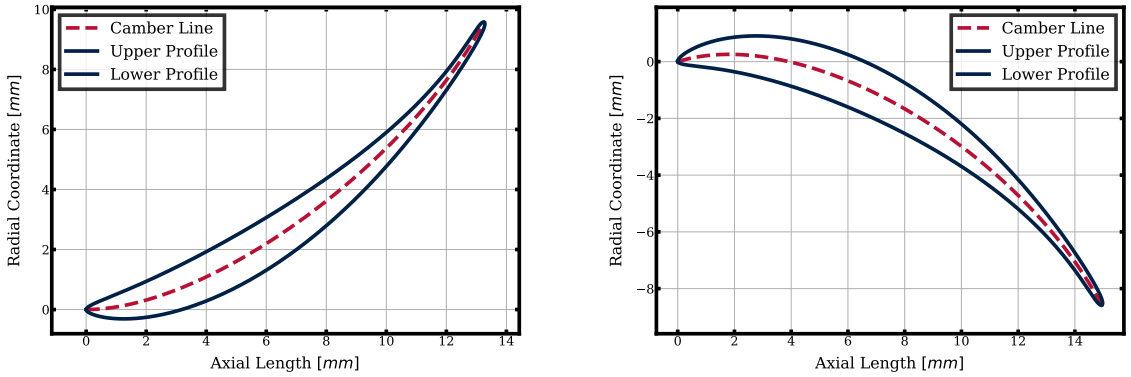

(a) Stator (b) Rotor

Figure 3.1: 2D Blade Sketches for the first stage

We must then proceed to the radial stacking of the blades to obtain a 3-D Blade profile. The blades where extruded to meet the hub and shroud contours and the flow path needed:

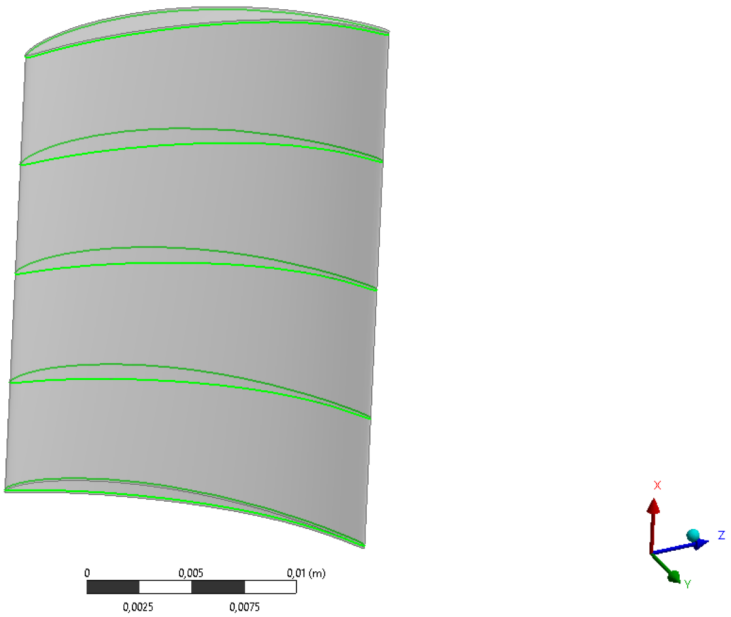

Figure 3.2: 3D Blade model by stacking

With the 5 radial sections of the blade, we created a 3D Blade. Now we have a complete and ready geometry to export to a CFD Simulation.

3.2 CFD Simulation

In this section, we discuss the details of the methodology followed to conduct an accurate numerical simulation. We will first start by defining the physical conditions to implement, we discuss the domain creation, the boundary conditions and the turbulence models to capture the flow behaviour around the boundary layer efficiently, we also discuss the computational mesh used for the parametric study and finally the overall solver's controls.

3.2.1 Physical Conditions

For our set of numerical simulations, we first make a regular numerical simulation with the optimal inlet and outlet parameters, the parameters are Total Pressure and Temperature at inlet, and Static Pressure at outlet. this is done for a fixed rotational speed at start (the design point), and then we do a multiple set of numerical simulations for different exit static pressure in hope to find the choking line for each rotational speed chosen. each time, we chose to fix one parameters and change the others. This yields in a smooth data a number conditions that can allow us to create the turbine performance map for a bunch of pressure ratios for example.

3.2.2 Computational Fluid Domain

For our performed simulation, the flow domain contains multiple blades that are set periodically around the flow path annuli therefore we have a rotational symmetry thus a periodicity of the blade arranging. A common approach in CFD calculations of turbomachinery components is to run simulations for only one blade passage rather than the entire annulus. This approach significantly reduces the computational time and even cost and provides us with the same results, this allows us to create even more finer cells for each blade passage to have a better catching around boundary layers. by assuming the periodic boundary conditions on the sides of the blade passages, the flow pattern repeats identically from one to next. This assumption is adopted when the blades around annuli are evenly distributed (which is our case by calculating the optimal pitch-to-chord ratio).

The inlet domain doesnt start right at the stator inlet nor the outlet artificial domain ends right at the rotor domain, to allow a better capture of the fluid flow, and to avoid having a reverse flow condition, we suppose a 1 Axial Chord added in the domain inlet and 1.5 Axial Chord added at the domain outlet. In the inlet, the extension permits the proper development of the flow before the fluid-blade interaction, thus reducing any influence of the boundary conditions on the upstream flow field and allows a uniform oriented velocity profile, this property is important for later inlet flow angles investigations. In the outlet, the domain extension permits the flow to exit smoothly, avoiding any artificial reflection of reverse flows that could disturb the numerical stability. This often happens at the limits of the turbine working range, where reverse flows occur, the extension of the domain helps to stabilize the simulation.

The fluid domain is shown in the figure below:

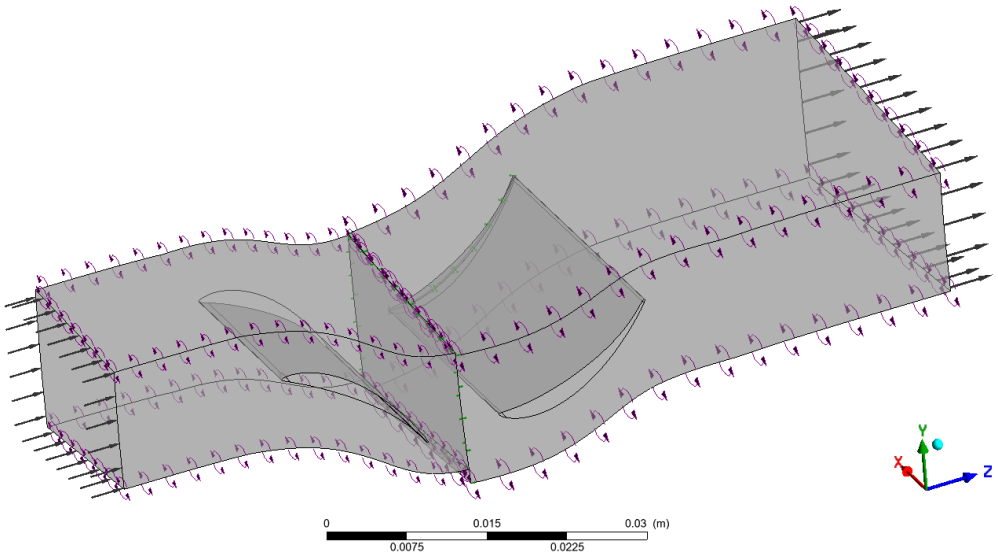

Figure 3.3: 3D Fluid Domain

. the length of the artificially added domains has a limit where it shows difference [7] therefore, our domain being already extended enough, we wont investigate the length of it in our parametric simulations

3.2.3 Solver Control Parameters

The simulation is run for a steady compressible and turbulent. It is modelled in the ANSYS CFX Turbomachinery tool, specifying Axial Turbine. since here the temperature varies, the Energy Model is setted to be ON and the $K-\omega SST$ (Shear Stress Transport) turbulence model is used as it is a widely recognized and used turbulence model for turbomachinery CFD simulation as $K-\omega$ can show some unsatisfactory results for high boundary layer pressure gradients. [8]

The K-ω SST Shear Stress Transport Turbulence Model

The model defines two equations, one for the turbulent kinetic energy k and the other for the viscous dissipation ε. these are defined as follows for the original K-ε model:

$$v = k^{1/2} \qquad l = \frac{k^{3/2}}{\varepsilon} \tag{3.3}$$

stress computation and the k- equation are the same as the original k-ε model but the ε-equation is transformed to an ω equation by changing it to $\varepsilon = k\omega$, its equation is written as:

$$\frac{\partial k}{\partial t} + \bar{u}_j \frac{\partial k}{\partial x_j} = P_k - \beta^* \omega k + \frac{\partial}{\partial x_j}\left[(\nu + \sigma_k \nu_t)\frac{\partial k}{\partial x_j}\right] \tag{3.4}$$

$$\frac{\partial \omega}{\partial t} + \bar{u}_j \frac{\partial \omega}{\partial x_i} = \alpha S^2 - \beta \omega^2 + \frac{\partial}{\partial x_j}\left[(\nu + \sigma_\omega \nu_t)\frac{\partial \omega}{\partial x_j}\right] + 2(1-F_1)\sigma_{\omega 2}\frac{1}{\omega}\frac{\partial k}{\partial x_i}\frac{\partial \omega}{\partial x_i} \tag{3.5}$$

3.2.4 Mesh Generation and Grid Independance study

3.2.4.1 Mesh Generation

To obtain a mesh that aligns with the flow and turbulence model needs, we use ANSYS CFX TurboGrid to generate a structured mesh that transforms the computational domains into cells, this is done by firstly importing our Geometry into ANSYS Workbench DesignModeler, where the Hub, Shroud, Inlet, Outlet and blade contours are defined with the correct blade set of the whole turbine, and then exported to TurboGrid to generate a structured hexaedral mesh with respect to the blade geometry and aligns with the flow direction. Down below is a Mesh Generation for a Rotor with tip clearance.

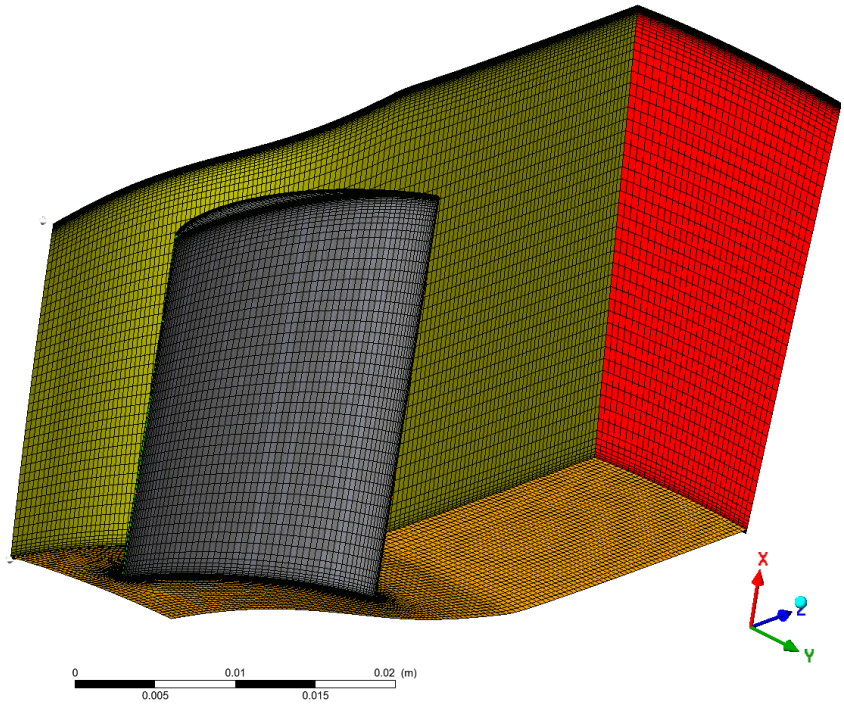

Figure 3.4: 3D Hexaedral Rotor Mesh

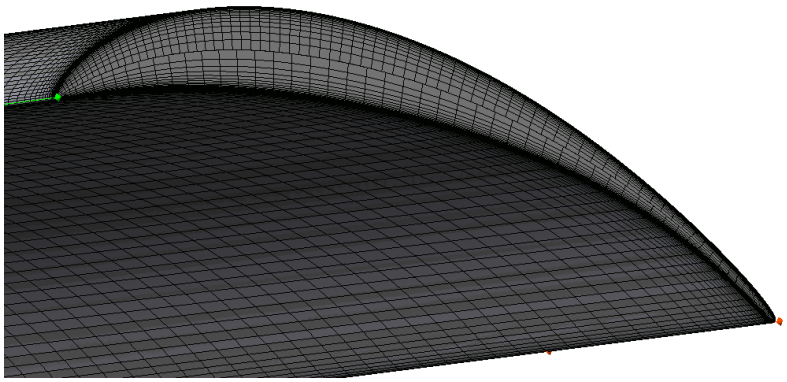

Figure 3.5: Refined Mesh for Tip Clearance

We imposed a 1 % of blade span for shroud tip clearance at the Rotor, therefore having a refined mesh at this location as shown in the figure above.

3.2.4.2 Grid Independance Study

In our study, we tried several spacial discretisations and obtained results for multiple cases regarding the number of cells for the same working conditions, which is what we call the mesh-grid sensitivity to ensure that the numerical simulation is independant of the mesh number of cells (or density). The process involves running simulations for the same working conditions but by increasing the levels of mesh refinement from coarse to fine. We take some key output simulated values and compare them. if the difference between a coarser mesh and a finer mesh becomes insignificant, then we consider that adding the number of cells useless, and gain computational cost and time by choosing the coarser mesh. The results of this process is discussed later on.

3.3 Rotation Modeling Approach

For a turbomachinery component and especially axial turbine, several approaches can be taken such as Frozen Rotor, Moving Reference Frame or Stage Mixing plane, each got its properties. we used here the stage mixing plane approximation. It creates a numerical interface between stationary and rotating elements. The main purpose of this interface is to average the flow variables in the circumferential direction, thus allowing the simulation of multiple cascade rows with different rotational frames without modeling the entire geometry but rather simplifying it to one blade passage only. the stator being a fixed component, transfers the circumferentially averaged properties of the flow to the rotor, the rotating component, which is why we called ”Mixing” as the rotor recieves the mixed profile as it’s inlet condition. This method allows us to reduce the computational time. By adding the condition of only simulating one passage and applying stage mixing plane, we get a good cost-efficiency ratio. The modeling of the interfaces and the boundary conditions are defined in the figure down below, the boundary conditions are explained in the next section.

3.4 Boundary Conditions

The surfaces of the blades, hub and shroud of the stator and the rotor hub are defined as No-slip walls, but the Rotor shroud is defined as a counter-rotating wall (to take in consideration the tip-clearance presence, and taking the effect of the stationary shroud.), The interface linking the stator to the rotor, is defined as a stage mixing plane as explained before. The figure below shows the boundary conditions: The rotor and stator interfaces are defined as periodic (taking in account the whole blade row). We specify at the Stator inlet a total temperature and total pressure, and at the Rotor outlet the estimated static pressure. The rotor rotates at the assignated design speed, the rotating speed and outlet static pressure are parameters we change at every simulation to construct the turbine performance map. The fluid used is the Air as an ideal gas.

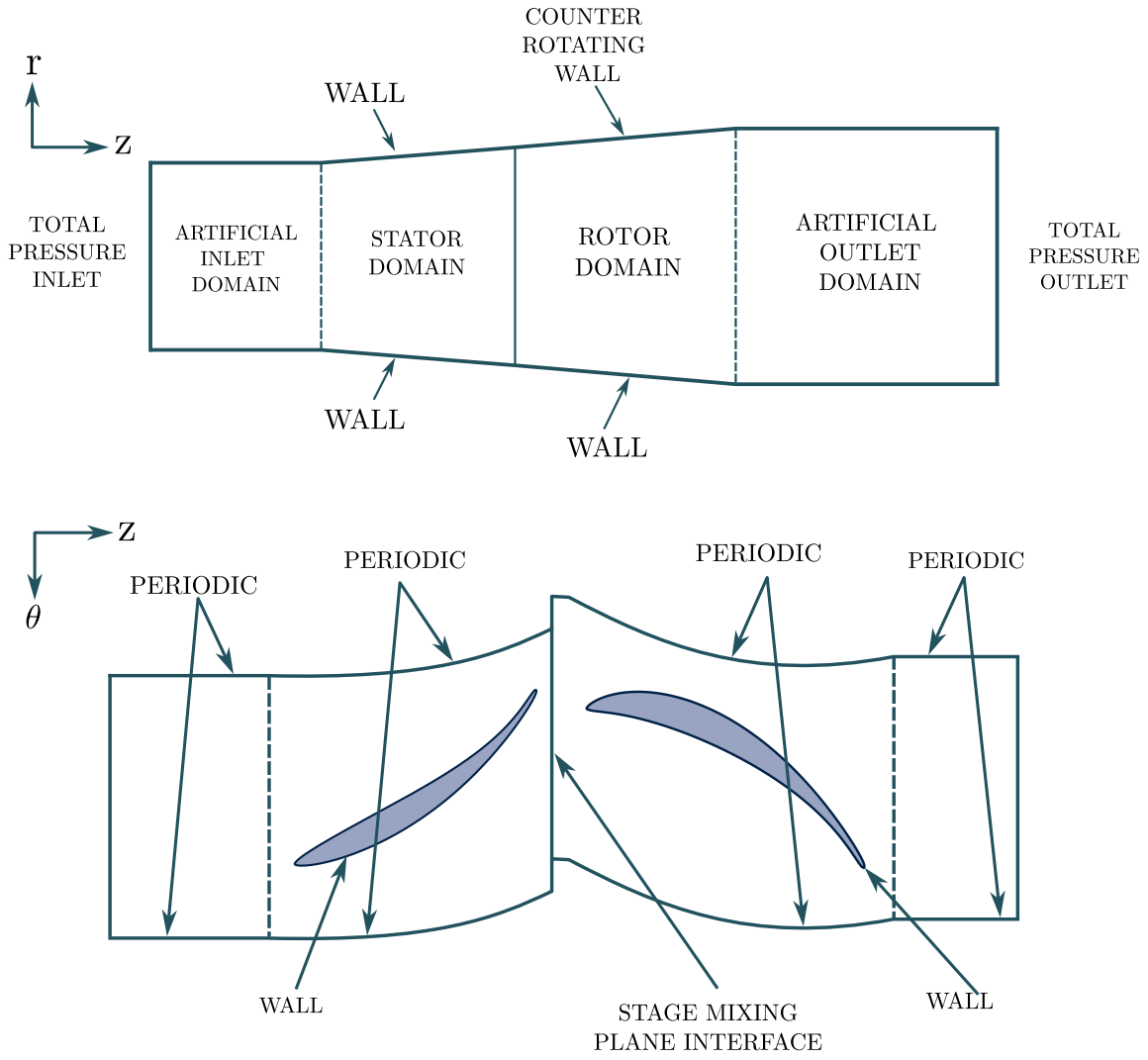

Figure 3.6: 3D Fluid Domain

Now that our set of solver control parameters are defined, we can start performing the numerical simulations, but in order to again, optimize the calculation running time, we must define an important convergence criteria. It is possible to admit the residuals as the convergence criteria, therefore, in extreme conditions they can produce some oscillations that disturb the numerical stability of the simulation, therefore, we take another convergence criteria, which is the mass flow, an expression was inserted in the CFX definition file to monitor the mass flow at the inlet and the mass flow at the outlet, and once these two values become indistinguishable, we consider that the simulation converged efficiently. Despite the residuals not reaching the convergence set. The details of running the simulations are explained in the next section.

3.5 Initializing and running the simulation

To have a better efficiency in the calulation, we start by defining one definition file running with Upwind advection and first order turbulent numerics schemes, by imposing a residuals of 10^{-4} for a maximum iterations of 100, generally, the convergence is reached very quickly. Then, we impose a high resolution advection and turbulence numerics scheme with a 10^{-5} convergence criteria and for a maximum number of iterations of 400, the convergence is generally reached

within this range. The solution of the upwind simulation is defined as an initial value for the high resolution simulation, therefore we provide a numerical stability at first to give the high resolution scheme a good initial value to perform and refine the solution.

Generally, for the high resolution scheme near the working conditions, the simulations run normally and converge fast. Therefore for the chocking conditions, oscillations start happening, as decided before, we decide the mass flow as our convergence criteria in this case.

We could define the high resolution scheme as 10^{-4} like we did for the upwind scheme, but in what we saw, no case of mass flow converged before the residuals reached this criteria, but rather, the mass flow converges generally between 10^{-4} and 10^{-5} residuals value (for extreme conditions).

3.6 Conclusion

In this chapter, the complete workflow of the designed turbine and simulation preparation was detailed. Starting off with the geometrical construction of the hub, shroud constructions and blade profiles by the stacking methodology to obtain the 3D model shape to export to the ANSYS TurboGrid mesh tool where we defined a structural mesh with careful attention to it's quality ensuring the necessary refinement for the efficient working of the turbulent models especially near boundary layers and tip clearance locations.

We explained how the extension of the inlet and outlet domain were made to ensure the numerical stability. with the computational domain defined, we detailed the approach adopted to model the interface between the rotor and the stator to capture the rotating effects and explaining why we adopted the stage-mixing lane approach.

Finally, the appropriate boundary conditions were implemented according to our design, by defining the inlet and outlet parameters and explaining the approach to realise the turbine performance map.

A final point was given to the simulation run methodology and explained how we perform them in a two steps, first with a low order for numerical stability, and secondly with a high order to refine the solution.

We can now explore the results given by the numerical simulations.

Chapter 4

Numerical Results

Before starting, we should In this chapter, we will try to do a summary of what numerical simulations gave us of exploitable data of our designed turbine. First of all, we show the results given by the grid independence study:

4.1 Mesh Grid Independance

The fixed parameters for the were the rotational speed, set to 38000 RPM, the total inlet temperature 1400K and static outlet, estimated to 5.01 bar. The mesh grid sensitivity study give us the following table:

Table 4.1: Values of Pressure Ratios P_r for a set of computational grids

Grid	Number of Cells	Pressure Ratio
G1	102510	1.9910
G2	201783	1.9905
G3	398430	1.9876
G4	599400	1.9867
G5	804475	1.9865
G6	1023551	1.9865

The values obtained for several grid meshes, ranging from 200K components to One million, give us an insight on the calculation to run. We have to note the simulation running time increasing significantly from the first case to the last case, thankfully, this study showed that for a 600K grid mesh, the values of pressure ratios are almost indistinguishable from the previous grid. Therefore, increasing the number of cells after 600K becomes insignificant and counterproductive. we gain nothing but more simulation time. Therefore the 600K grid is adopted for the rest of the study. Despite a relatively longer simulation time compared to coarser grids.

The simulations for coarse meshes can take up to five minutes, where the simulation on the very fine meshes can take up to 30 or 40 minutes to perform (Double running)

For our grid, the mean simulation time is around twelve minutes. Which is a good compromise.

The simulations are run on an I9-14900HX 5.6gHz, 36GB RAM.

4.2 Results for the turbine stage working conditions

As a reminder, the design conditions of the turboprop are as follows:

- Flow rate $\dot{m} = 8.5kg/s$
- Entry Total Pressure $P_{t_{in}} = 12Bar$
- Entry Total temperature $T_{t_{in}} = 1400K$
- Total-to-total Pressure ratio of 9.5
- The rotational speed $N = 38000rev/min$
- The maximum allowable speed at the mean-radius is $U_m = 420m/s$
- The total-to-total efficiency $\eta = 90\%$

The total pressure ratio is chosen to be equal between stages as follows:

$$Pr_{stage} = Pr_{overall}{}^{\frac{1}{n}} \tag{4.1}$$

With n being the number of stages. here n is equal to 3, therefore the total pressure ratio of all stages is equal to 2.11

As we define a static outlet boundary condition, we must evaluate the static pressure outlet in our design. Having in our calculations found the total pressure at the exit of all stages, and the critical Mach numbers after the rotor blade cascades. we use the expression used by E. Baksharone to calculate the static pressure:

$$P_{t_{static}} = P_{t_{exitrotor}} \left(1 - \frac{\gamma - 1}{\gamma + 1} {M_{cr_{exit}}}^2\right)^{\frac{\gamma}{\gamma - 1}} \tag{4.2}$$

We get these results for the outlet static stages:

Table 4.2: Pressures and Mach numbers at the stages exits

Stage	1	2	3
Total Pressure outlet	5.66	2.67	1.26
Critical Mach Number	0.45	0.48	0.51
Outlet Static Pressure [bar]	5.01	2.33	1.08

We are now set to see the results for our stage simulation. And we also have the results of previous stages if needed to simulate other stages, we perform one numerical simulation with the Total pressure and temperature as defined in the design point, and the pressure outlet as calculated during the design. which was found to be $P_{static_{out}} = 5.01bar$

Here is a brief summary of the found results for this first stage simulation:

Table 4.3: Summary of simulated values

Mass Flow [kg/s]	Total Pressure Ratio P_r	Total temperature Ratio T_r	Efficiency [%]	Shaft [W]
11.0307	1.9876	1.19	90.95	2 505 070

We also get the plots for Mach numbers, plots of velocity stream lines, static pressure and Mach Numbers contours.

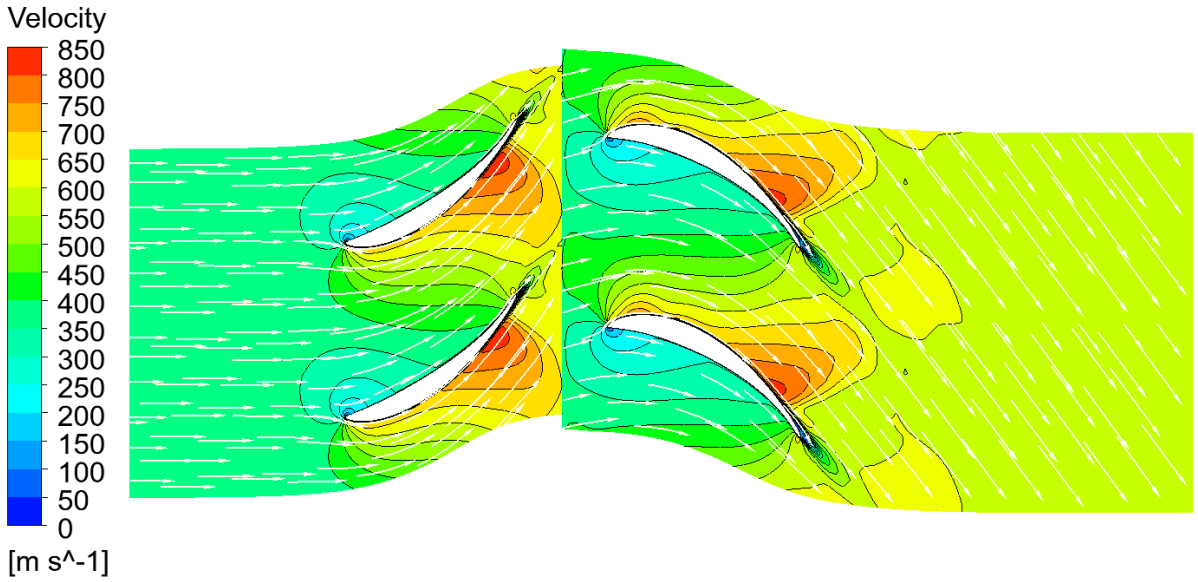

Figure 4.1: Velocity streamlines in the axial direction across the passage

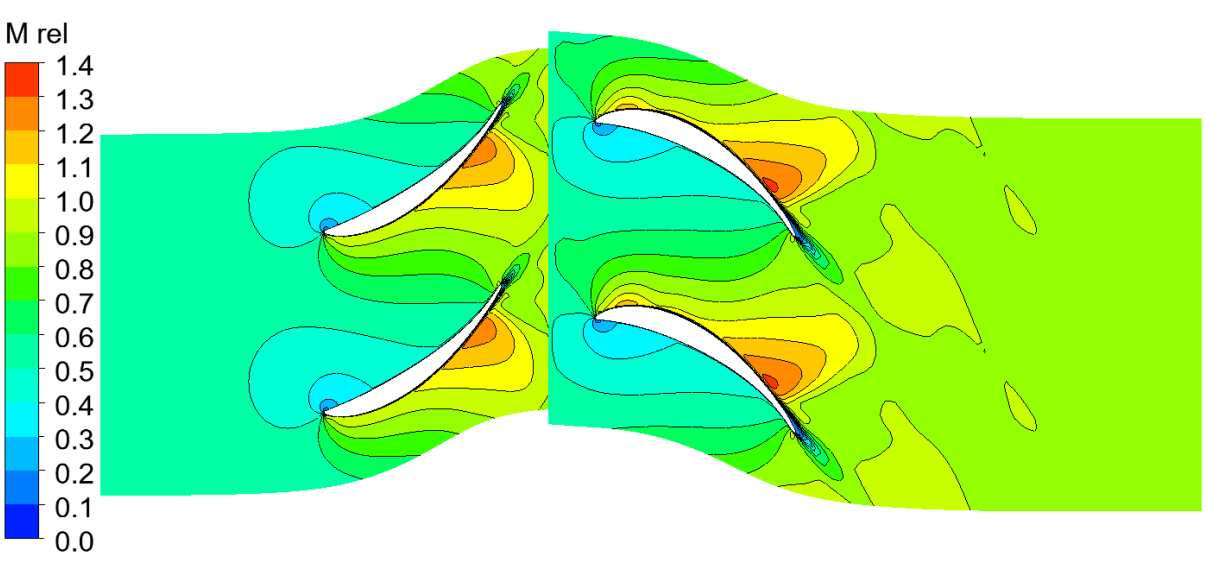

Figure 4.2: Relative Mach Numbers values

We also get the pressure contours around the blades:

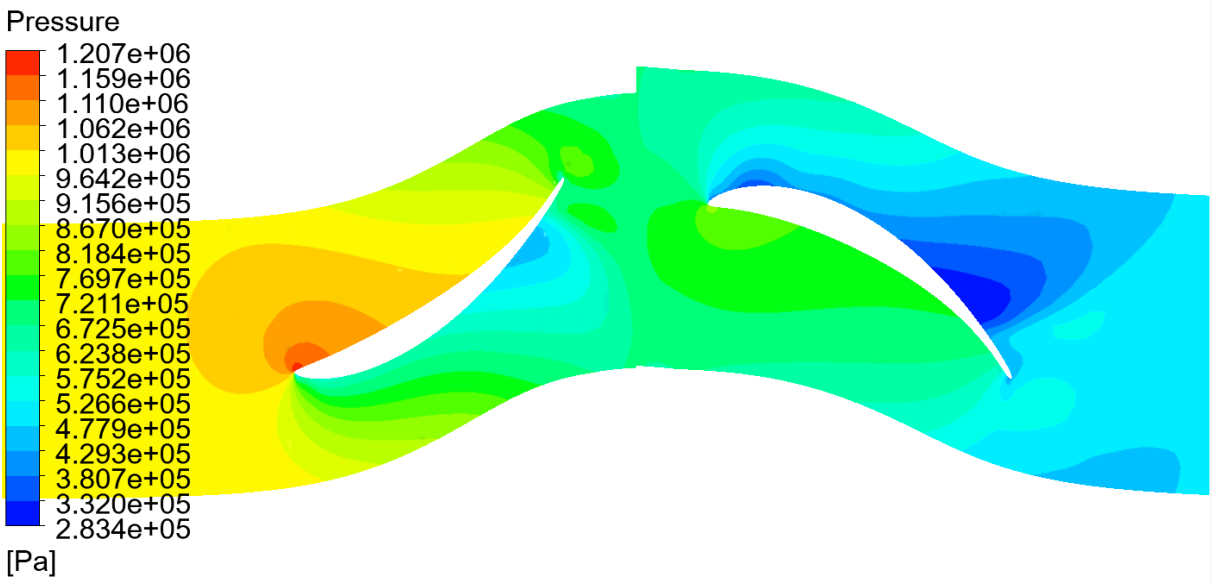

Figure 4.3: Static Pressure evolution

The first figure demonstrates the the stream lines of absolute velocity across the blade passage, as designed, the flow enters the domain with a speed between 250 and 300 m/s and accelerates through the stator, reaching around 600 and 650 after the blade exit, as calculated in the velocity triangles of the stage design. The velocity increases as logically as the stator cascade rows guide the flow to the rotor. The velocity component is normal to the boundary since we defined an 0 inlet blade angle, thus we can see the flow being smoothly guided. Through the rotor, the velocity is redirected by the rotor blades after which the velocity decreases slightly, indicating the occuring of the energy extraction process.

The figure shows a smooth evolution of the flow across the two blade cascades with no visible flow separation or backflows, showing a relevant numerical simulation.

The second figure presents the mach number across the blade passage (important for the study of the rotor, a component in the relative reference frame). Before the rotor, we can see an increase in the absolute mach number from the entry to the exit of the stator. For the rotor the relative Mach number increases significantly, indicating that the relative speed for the rotor, increases from the inlet to the outlet. This aligns perfectly with the velocity triangles of the axial turbine, where the absolute and relative mach numbers increase through the stator and the rotor respectively.

The summarised values of Mach Numbers are listed below, for the leading and trailing edges:

Table 4.4: Relative Mach Numbers before and after blade rows

Component \ Mach Number	Inlet	Leading Edge Cut	Trailing Edge Cut	Outlet
Stator (Abs)	0.5142	0.5130	0.9469	0.9052
Rotor (Rel)	0.5455	0.5585	0.9392	0.8529

This table shows us that, according to our design point, we have no situations of supersonic flows before the and after the blades, at the throat passage, therefore we are in the subsonic range where where, the turbine can operate.

The figure 3.3 displays the mach static pressure distribution across the blade passage, we take the static pressure here as it is more significant to present it for the stator blade, since for total pressure, it practically remains the same. we can see a smooth evolution of the static pressure from inlet and outlet of the stage. Therefore a local decrease of the pressure at the suction side of the rotor. this can be investigated in a further work regarding the aerodynamic of our blade.

The numerical simulation give us a good efficiency, close to the design point (90 %) therefore, the mass flow has a 20 % different value, this can be due to the estimated total loss at the stator that affects the blade heights. Nonetheless, this should be investigated in future work to get a closer value to the design point. We can here try some initial approaches, varying the aspect ratios to see how it can perform. The next section presents two cases of varying the aspect ratio, one by increasing both our initial aspect ratios, the other by trying a correlation given by Marco Gambini in his turbomachinery book.

4.3 Aspect Ratio correlation

In this section, we will try the correlations given by Marco Gambini [9], that starts by defining a coefficient λ that is the ratio between the blade hub diameter and blade tip diameter, with the blade heights known, we can easily calculate this ratio, then we get this ratio:

$$\lambda = \frac{D_h}{D_t} = \frac{1 - \frac{h_b}{D_m}}{1 + \frac{h_b}{D_m}} \tag{4.3}$$

use it for two correlations one concerning the stator and the other one concerning the rotor, as follows:

$$AR_{stator} = -11.48\lambda + 11.39 \tag{4.4}$$

$$AR_{rotor} = -12.44\lambda + 12.59 \tag{4.5}$$

This results in significantly lower and closer axial chord values, therefore an ”artificially” radially longer turbine, or rather, compact.

Table 4.5: Axial Lengths changes

Stage	Component	Initial	Correlated	Percentage of decrease
1	Stator	15.98	10.64	33 %
	Rotor	17.21	9.29	46 %
2	Stator	20.74	11.35	45 %
	Rotor	23.37	10.43	55 %
3	Stator	29.32	12.82	45 %
	Rotor	34.07	12.36	63 %

The values of the axial chords decreased significantly at around 30 to 60 %, and now we have a shorter axial chord of rotor compared to stators, subsequently, we have an overall higher number

of blades.

Therefore we obtain the following results:

Table 4.6: Summary of simulated values

Mass Flow [kg/s]	Total Pressure Ratio P_r	Total temperature Ratio T_r	Efficiency [%]	Shaft [W]
12.003	1.8337	1.1725	92.74	2 544 980

The results given show an even higher mass flow rate, and a lower pressure ratio, further than the design point (2.11). Therefore this correlation is not suited for the design of our turbine.

4.3.1 Results for increasing the actual aspect ratio

We tried increasing the aspect ratio of both stator and rotor to view its effect on the turbine performance. Therefore it gave slightly lower values. Therefore, it is insignificant to use different aspect ratios for now. The remaining study is conducted with the 600K mesh cells and the first defined aspect ratio.

4.4 Performance Map

Before initiating this section, we shall define a key notion for turbomachinery performances

4.4.1 The choking line

The choking line is a flow condition where the mass flow rate reaches its maximum possible value for a given set of conditions (for our case, it is the total-pressure ratio, it can also be applied to temperature ratio). This state is not necessarily [**?**] harmless, but where there is simply no more improvement of the value of mass flow. This following figure shows a typical turbine map by the pressure ratio as function of the mass flow for several speeds.

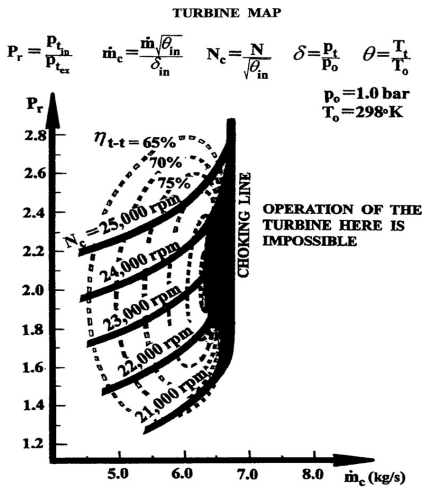

Figure 4.4: Typical Turbine Performance Map

Our goal is to determine the choking line for our turbine stage. This is done via a set of numerical simulation as follows: we fix the inlet total pressure and temperature, and a rotational speed, then, for each simulation we vary the pressure static outlet, providing us, for each simulation a mass flow rate and a total pressure ratio, when the simulated speeds allow us to create a relevant performance curve, we change the rotational speed and redo the same calculations. we then the performance map and show the choking line for a number of rotational speeds. in total, we did the calculations for four rotational speeds, each carried around 15 simulations, in total, for this section around 60 simulations were performed, thus we obtain the following map for 38000RPM, 34000RPM, 30000RPM and 26000RPM

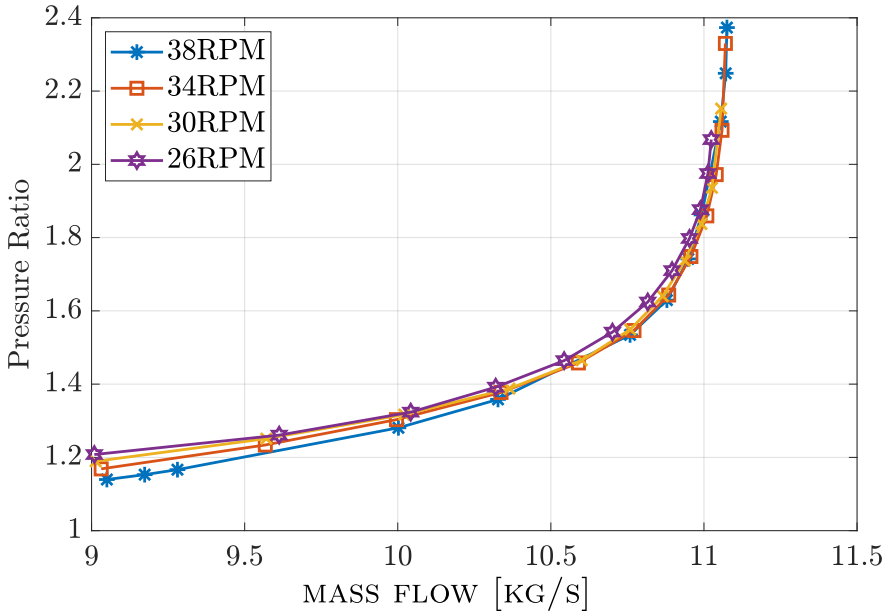

Figure 4.5: Turbine Performance with Pressure Ratio

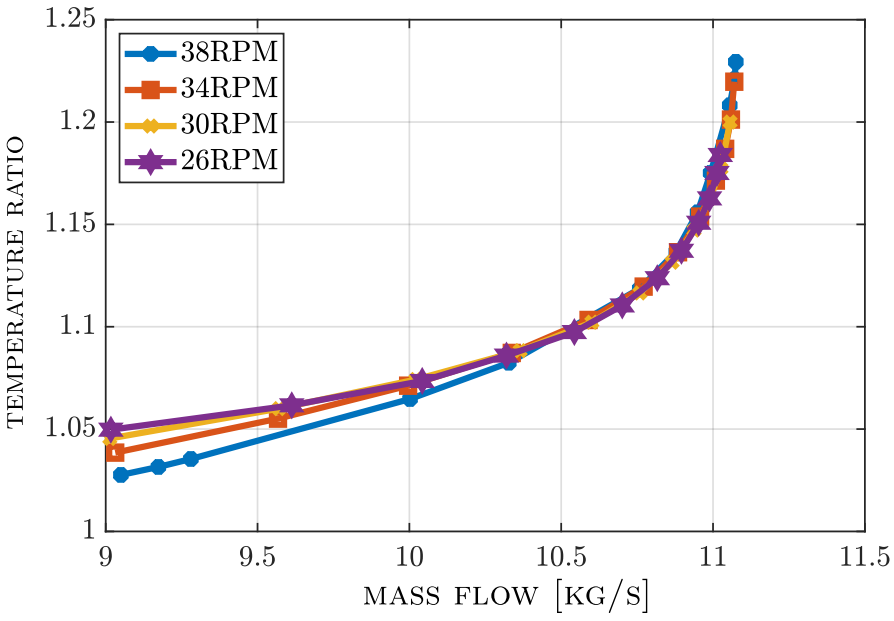

Figure 4.6: Turbine Performance with Temperature Ratio

4.4.2 Map performance analysis

The two above figure show us the tendency of the turbine for several pressure ratios, as function of the mass flow and the rotational speed. We can notice that it is the same pattern: for low mass flows, there is a small yet notable difference of the pressure ratio of all the rotational speeds, with the higher speed having the lowest pressure ratio and the lower speed having the higher pressure ratio. the increase of the mass flow is accompanied by the gradual increase of pressure ratio, until a certain point, where the mass flow reaches 11 (a small value above it), the pressure ratio keeps increasing without a notable difference of the mass flow, this is the choking line that we tried to show here. Therefore we can say that for our turbine, the choking line is at 11 kg/s.

We can also read the values with the efficiency, we can get the following graph:

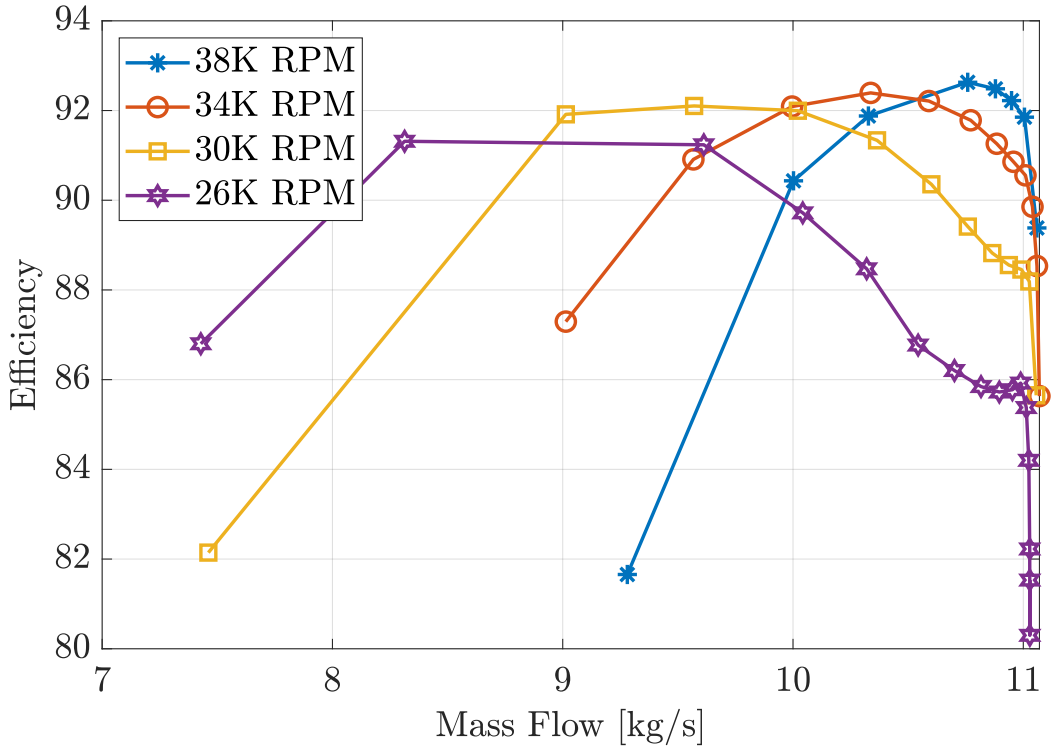

Figure 4.7: Efficiency evolution for several rotational velocities

The figure above displays the efficiency values as function of mass flow, for a set of rotational speeds, we can clearly see the tendency shown by all the four curves that the efficiency grows with the mass flow, until it reaches an optimum where it starts to shift to lower values, that maximal value signifies the reaching of the choking line, the values keep dropping until around 80 % (for the worst case). therefore we can see that the 38K RPM case has the highest optimal efficiency (around 92 %).

We can also see that practically all the efficiencies start to fall off right after reaching the choking line of near 11kg/s. We said earlier that the choking line is a harmless mechanical state, therefore it is not suggested to operate the turbine in these conditions as we get a significant drop of the machine efficiency.

Finally, for this step, we can give values of the shaft, in the following graph

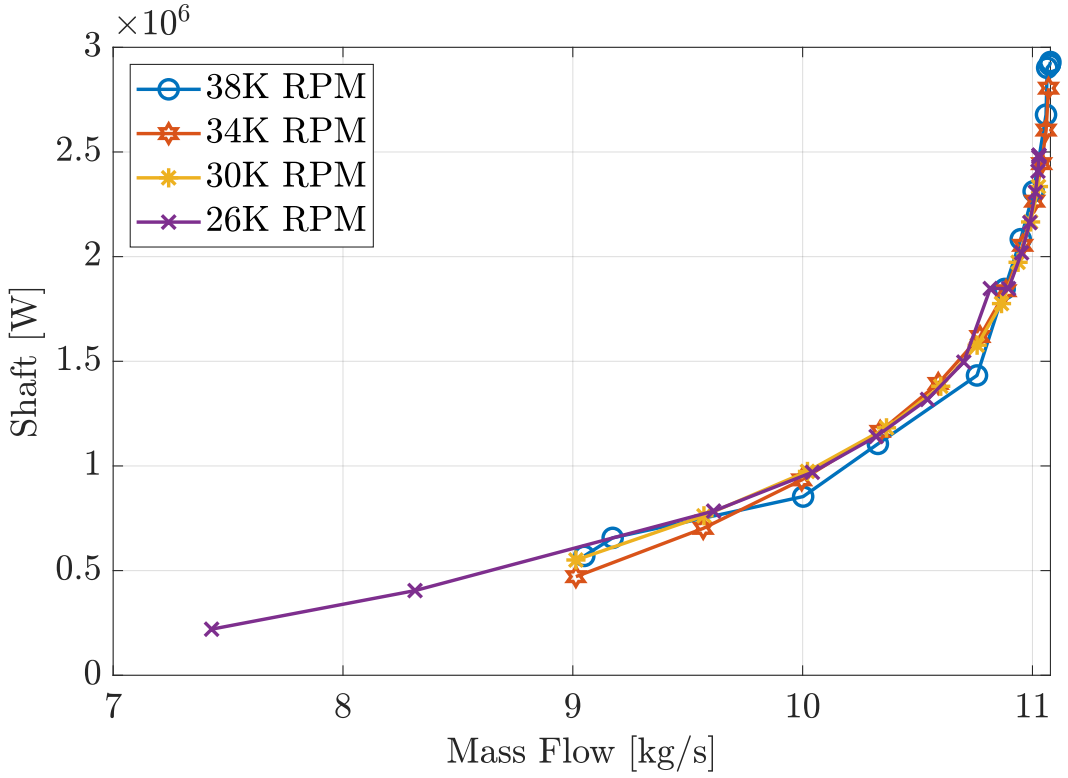

Figure 4.8: Shaft evolution for several rotational velocities

A property to retain from this graph, is that, shaft increase gradually for all rotational speeds, until reaching the choking line and a phenomenon happens there, the shaft stops increasing. the plot doesnt show it much since both shaft and mass flow are chocked, therefore we know now, the behaviour of the shaft at the choking line.

4.4.3 Conclusion

The turbine performance map has been created for the first stage (considering it for the turbine by extension as a preliminary approach) and we we could catch data that translates well the stage behaviour for multiple set of parameters. First of all, we defined the choking mass flow value to be around 11 kg/s, after which, no higher value of pressure ratio or temperature ratio will provide any significant change in the mass flow. We also saw how stage efficiency behaves a the chocking condition that is by decreasing gradually until a sudden drop of efficiency, making the choking line a state that should be avoided thermodynamically. Finally we saw the shaft work behaviour and how it matches the choking state with the mass flow.

In the next section, we decided to perform final numerical simulations of the full turbine, to have a general idea, and to validate the notion of taking only one stage as a base of the build of the performance map.

4.5 The Three Stage Turbine Full Turbine Simulation

To finish off this work, we performed a final set of numerical simulations, 10 in total for the whole blade geometry, where the thermodynamic boundary conditions were fixed to the design point, but we changed the rotational speed to get a better insight on some parameters at different speeds. Therefore, we obtain these plots:

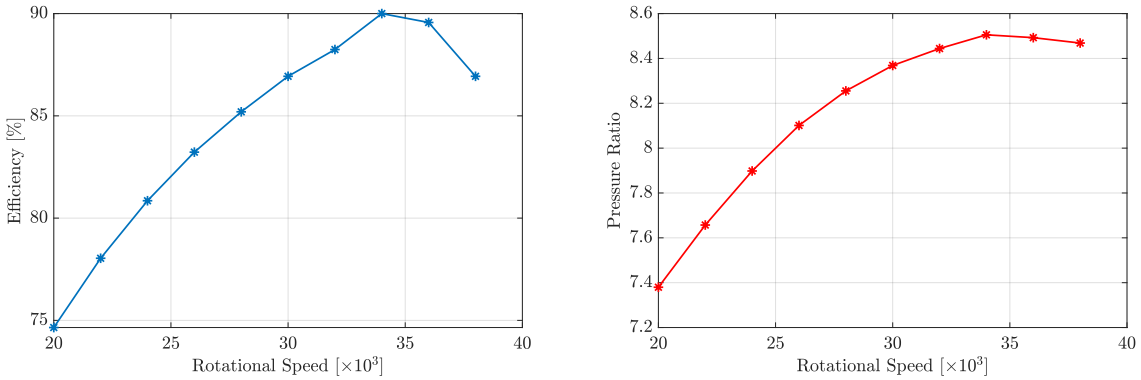

(a) Efficiency (b) Pressure Ratio

Figure 4.9: Graphics of efficiency and Pressure Ratio by varying the rotational speed

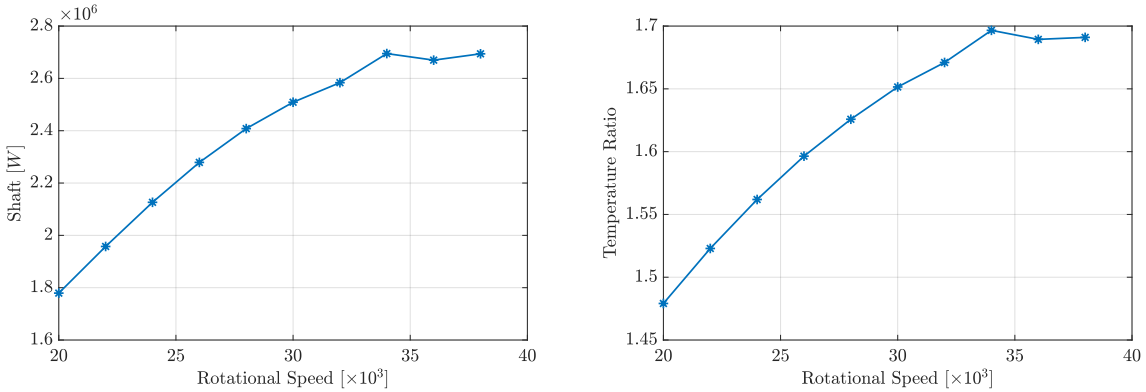

(a) Shaft (b) Temperature Ratio

Figure 4.10: Graphics of Rotational Speed and Temperature Ratio by varying the rotational speed

4.5.1 Analysis

We can see in the above figures, the same tendency for the four selected parameters to measure, starting from the low rotational speed, the parameters increase significantly by increasing the speed, until reaching an optimum which was 36K RPM, where the values start to slowly drop.

Also, for the whole turbine, we can investigate the three stages one by one to extract some key informations.

Table 4.7: Summary of simulated values

	Mass Flow	P_r	T_r	Shaft	η
1	11.0328	2.1331	1.2102	2693980	89.093
2	11.0333	2.0375	1.1954	2096860	88.4781
3	11.0377	1.9321	1.1693	1556780	84.3759

We can extract some parameters from this as follows:

First of all, the mass flow for all the three stages is verified, therefore, the continuity is satisfied, when it comes to pressure ratios, we can see a slight drop from stage one to stage three, even though during the design, we imposed an equal pressure ratio for all stages, there is some losses, but the methodology is close to real pressure ratio, especially for the first stage. Next, the temperature ratio, that is decreasing from first stage to last stage, this is especially due to the worksplit, since the first stage beneficiated from almost 39 % of the work, the enthalphy drop is bigger and the total temperature variation is more important, this property is even more verified in the shaft, the first stage has a 42 % amount of the total shaft, 33 % for the and 24 % for the final stage. This reduced work split for the lower pressure stages is accompanied in a loss of efficiency, as a reminder

$$\Delta H_{T1} : \Delta H_{T2}; \Delta H_{T1} = 39; 33; 28 \qquad (Design) \tag{4.6}$$

$$\Delta H_{T1} : \Delta H_{T2}; \Delta H_{T1} = 42; 33; 24 \qquad (Simulated) \tag{4.7}$$

These values are close to the design definitions, therefore the methodology provides a good preliminary approach

We can also see the velocity contours of the three stages showing the smooth flow of the fluid from one passage to another in respect to how the camber line was constructed, to ensure the perfect positioning of the blade to welcome the flow.

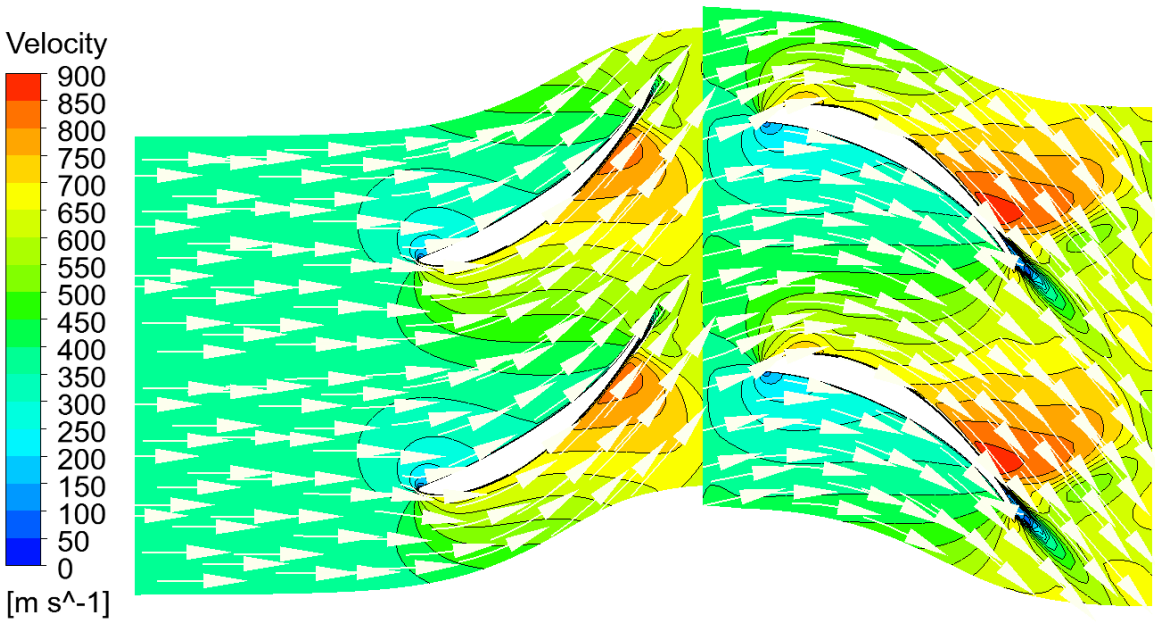

Figure 4.11: Velocity streamlines for the first stage

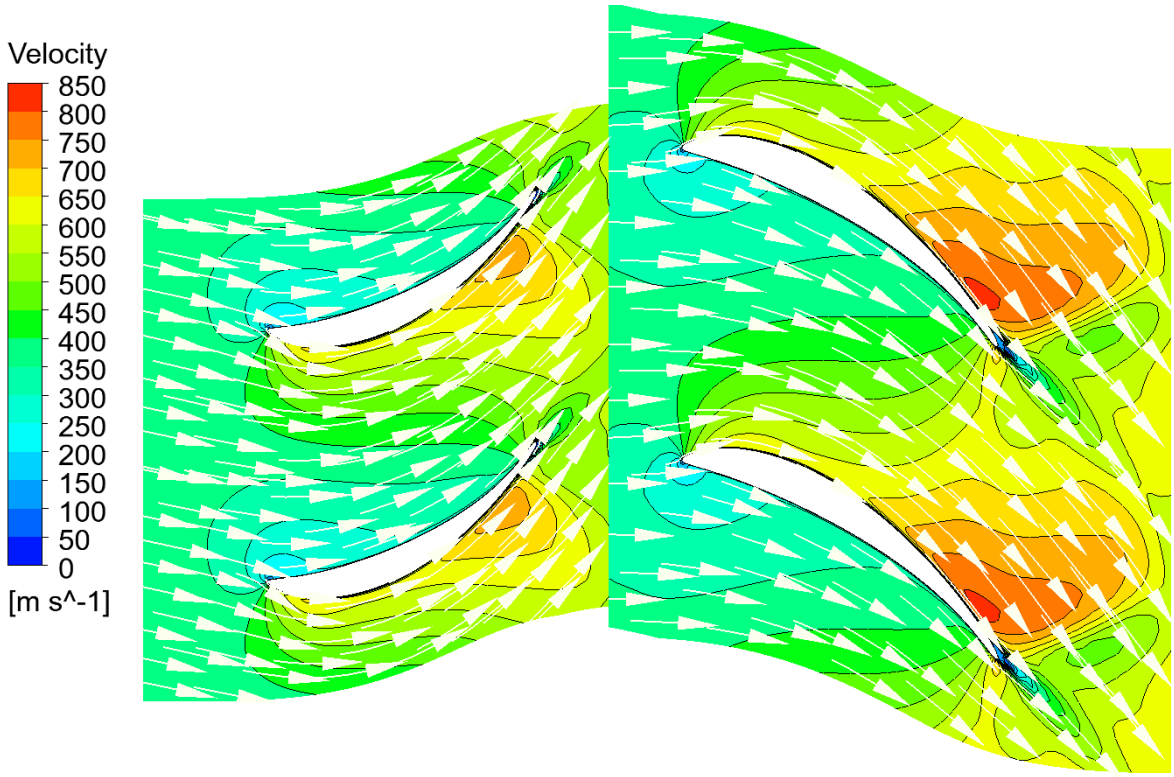

Figure 4.12: Velocity streamlines for the second stage

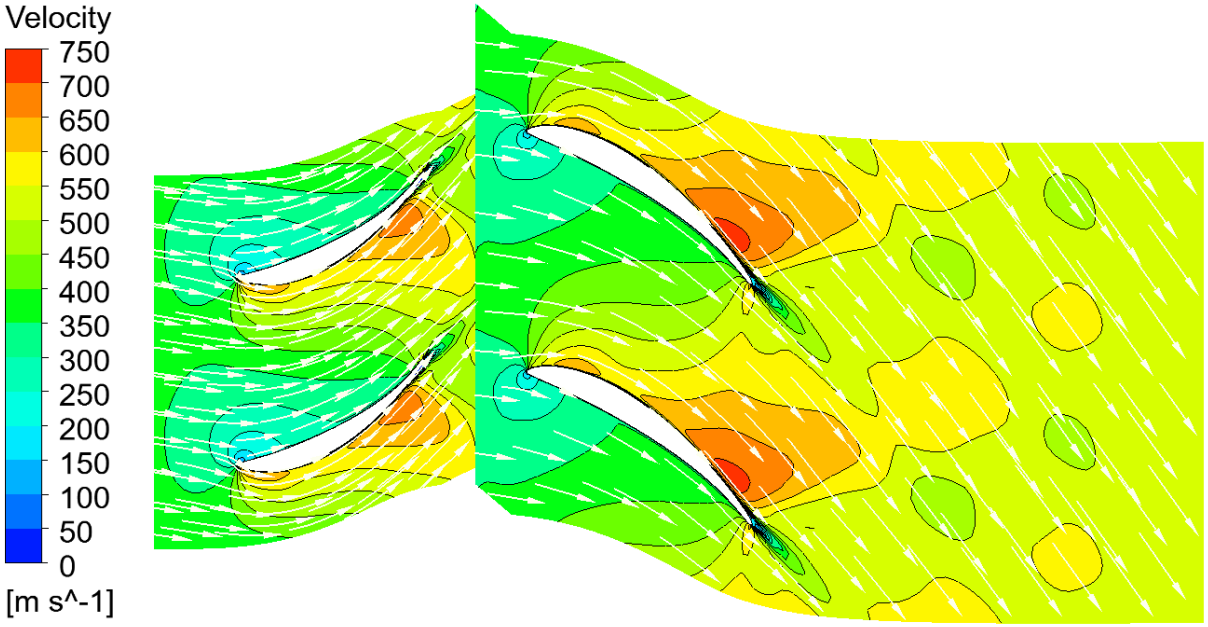

Figure 4.13: Velocity streamlines for the third stage

As shown in the above figure, for the second and third stages, the flow respects the entry of the third stage, or in another way, the blade was constructed in a way to optimize and to optimally recieve the flow from the preceeding component, or stage.

Chapter 5

Conclusion

This work carried a detailed methodology followed to the simulation of an axial-flow turbine, by using the data given by the algorithm followed by the code we wrote for a complete turbine design for given conditions and limitations. We started by showing the details of our design in a geometrical way, axial lengths, axial gaps and most importantly the blade geometry and 3-D blade profile construction, and the export methodology to generate a turbine hexaedral mesh in turbogrid for an optimized numerical simulation. we discussed in detail the methodology followed to set up the simulation, the approach followed to model the rotation of the rotor in steady state and how the interfaces and boundaries where defined, explaining why whe chose the stage-mixing plane and how it ended up being a good choice. we talked about how we defined the periodicity of the flow domain to lower the cost of the simulation, we also detailed the methodology followed to define and reach smoothly the convergence of the simulations.

We then explained the choice of mesh chosen regarding to the mesh grid independance to again, make an efficient numerical simulation and safe calculation time.

In the physics of the turbine, we showed the methodology followed to construct the axial turbine performance map, which was by varying and fixing a set of parameters for every iteration to have enough data to construct our map and define the choking line and the turbine extreme working conditions.

We also investigated the influence of the aspect ratio on our turbine by trying two other configurations.

We also performed, in the end the numerical simulation for the whole turbine to validate the approach of only modeling one stage of the entire turbine, we investigated the parameters of every stage mostly the work split, as it is an impotant factor in the preliminary design.

The followed CFD approach helped us understand more on what was built in the preliminary theoretical design approach, and allowed to to explore the mean-line model in depth by applying it in high-fidelity environment which was the CFD.

This work will be carried on to optimize further more the design of our turbine by implementing the CFD approach to it for future research.

Bibliography

[1] E. Baksharone, Principles of turbomachinery in air-breathing engines, Tech. rep.

[2] S. Bahamonde, M. Pini, C. D. Servi, A. Rubino, P. Colonna, Method for the preliminary fluid dynamic design of high-temperature mini-organic rankine cycle turbines, Journal of Engineering for Gas Turbines and Power 139 (8 2017). doi:10.1115/1.4035841.

[3] Z. S. Seyed Ehsan Hosseini, Saeid Jafaripanah, Numerical simulation and aerodynamic optimization of two-stage axial high-pressure turbine blades (2024).

[4] E. L. Z. Vinícius Guimarães Monteiro, Numerical simulation of performance of an axial turbine first stage (2012).

[5] M. K. K. Nader Elqussas, Axial flow turbine aerodynamic shape design optimization (2021).

[6] R. Agromayor, L. O. Nord, C. Wieland, R. Pili, N. Siamisiis, H. Spliethoff, Efficiency correlations for off-design performance prediction of orc axial-flow turbines, Tech. rep.
URL `https://www.researchgate.net/publication/336769907`

[7] J. George, T. Basson, Design methodology of an axial-flow turbine for a micro jet engine, Tech. rep. (2014).
URL `http://scholar.sun.ac.za`

[8] H. K. Versteeg, W. Malalasekera, An introduction to computational fluid dynamics second edition, Tech. rep. (2007).

[9] M. V. Marco Gambini, Turbomachinery Fundamentals, Selection and Preliminary Design, 2012.

Chapter 6

Appendix

6.1 First Stage Stator Airfoil Coordinates

X Lower Profil	Y Lower Profil	X Upper Profil	Y Upper Profil
0		0.310191408654814	
0.00307202604626702	0.293310458807577	0.00303181636208318	0.327074177583028
0.0123135016856399	0.275551611714664	0.0121075093803536	0.344860288918069
0.0277999639314909	0.256991818821389	0.0271683372512807	0.363538047617108
0.0496164648986244	0.23773587155352	0.0481568108979434	0.383110875511428
0.0778560568486818	0.217897176938131	0.0750175700458442	0.403615718882807
0.1126176520687	0.197629262432462	0.107698638047716	0.425090408710419
0.15400426679587	0.177098394294454	0.146152055275187	0.447599597770289
0.202120754638498	0.156495829654041	0.190334797092527	0.471220765257915
0.257071542091224	0.13603593538837	0.240209477606575	0.496044068886602
0.318958312685183	0.115954712910795	0.295744908641748	0.522171520527585
0.387877675439023	0.0965084110780378	0.356916496311209	0.549715820360664
0.463918878420148	0.0779717579740808	0.423706434289757	0.578799337808058
0.547161580399574	0.0606362754306488	0.496103702410899	0.60955279612733
0.637673350820534	0.044811904237068	0.574104223461476	0.642110454983263
0.735507691525568	0.0308227671575153	0.657710409092985	0.676610987510964
0.840702436430734	0.0190023418911774	0.746930264065736	0.713198804532545
0.953278311355587	0.00969016497505104	0.841776292823352	0.752023730694203
1.07323661469296	0.0032355249586723	0.942265274473637	0.793233600723473
1.20055672540998	0	1.04841822674553	0.836967947737368
1.33519802238697	0.000336122165422836	1.16025600202129	0.883375528733924
1.47709881128228	0.00458947432114676	1.27779794614971	0.932608408913733
1.6261720920496	0.0131134692460083	1.4010638133392	0.984803382636418
1.7823048842469	0.0262635491222076	1.53007224569807	1.0400840199763
1.9453652174874	0.0443644659530604	1.66483173481206	1.09858970492292
2.11519918085764	0.0677244281045403	1.80534169507279	1.16045790589193
2.29161876447316	0.0966748189621391	1.95160293769603	1.22578099748563
2.47441786241187	0.131508199911233	2.10360019665632	1.29466494510358
2.66337412062104	0.172477693651256	2.26129904156745	1.36722677889942
2.85823754421186	0.219833878081899	2.42465627969487	1.44355474788182
3.05872278171555	0.273841148602387	2.59362694393882	1.52368921572906
3.26454238657154	0.334684439573491	2.76813057859604	1.60771342521229
3.47539522618628	0.402510399429281	2.94806266218467	1.69571005249411
3.690929465551	0.477518004169911	3.13333174740915	1.7876685803257
3.91079068278266	0.559835400528197	3.32381176533119	1.88360671051389
4.13462978473731	0.649512575611572	3.51933482733958	1.98357622835775
4.36207610338821	0.74658848888895	3.71971914324992	2.08759469046919
4.59269179576415	0.851181589732647	3.92481592904117	2.19555401779875
4.82607875601884	0.96326541028464	4.13440408925852	2.30744430686043
5.0618843854184	1.08267936311688	4.3481863192406	2.42334273018333
5.29954872620247	1.20960784921501	4.56604410957451	2.54293441871518
5.53880757351326	1.34363849845053	4.78753702445181	2.66645450006507

X Lower Profile (Cont)	Y Lower Profile(Cont)	X Upper Profile(Cont)	Y Upper Profile(Cont)
5.77920901942075	1.48467673015407	5.01238878338899	2.79377409888154
6.02013562215417	1.63286101475733	5.24046793445867	2.92448591024157
6.26135097320703	1.78764911841166	5.47124432554308	3.0588190540122
6.50236394060998	1.94890716983135	5.70442807259746	3.19655135894388
6.74273158649989	2.11639318806156	5.93967000237575	3.33752742406319
6.98204073009829	2.28979900225534	6.17658357259812	3.48161851094763
7.21992128457289	2.4687402623299	6.41473511391848	3.62873455122803
7.45596759312012	2.65287755018347	6.65372614016307	3.77870524156415
7.68979064234316	2.84184050454379	6.89314481980237	3.93135829382901
7.9210250568727	3.0352237459908	7.13256267522809	4.08652603382653
8.14934513671608	3.23257198062629	7.37152221861497	4.2440629491792
8.37442592077364	3.43343737971974	7.60957951120325	4.40379106759961
8.59595718824001	3.63736353893487	7.84629370483565	4.5655188401084
8.81365369370977	3.84387644429729	8.08122024102012	4.7290530800226
9.02725909387984	4.05248437549677	8.31391022151662	4.89420200511424
9.23654723644169	4.26268110838712	8.54391225279788	5.06077499926895
9.44130213316076	4.47397289837043	8.77079541662672	5.22855859053456
9.64133198865476	4.68586448868827	8.99413797100911	5.39733338067845
9.83646905019735	4.89786232004846	9.21352999371688	5.56687372970285
10.0265715782765	5.10947517591831	9.42857364812723	5.73694994176559
10.2115239589422	5.32021671165025	9.63888503196445	5.9073284861726
10.3912229881442	5.52962153830394	9.84410956267443	6.07775856560563
10.5655846974061	5.73723901170091	10.0439165164809	6.24798086540189
10.7345430696712	5.94263551131831	10.2380013612677	6.41772768507132
10.8980483484059	6.14539669481112	10.426088171879	6.58672295359529
11.0560698996402	6.34512515587005	10.6079271626047	6.75468668975767
11.2085870011994	6.54144902064277	10.7833039598747	6.92132836293309
11.3555866920869	6.73402305237134	10.9520414823391	7.08634757707774
11.4970649825955	6.92252650077814	11.1139981307619	7.24943783556933
11.6330252209917	7.10666335629542	11.2690684977285	7.41028772277859
11.7634766763013	7.28616214301447	11.4171835462869	7.56858236627193
11.8884343925538	7.46077446902734	11.5583092135423	7.72400596053008
12.0079175086786	7.63027471151117	11.6924462590183	7.87624297613794
12.1219438688603	7.7944623311477	11.8196335495045	8.0249765628561
12.2305324428783	7.9531578293117	11.9399432797631	8.16989313777534
12.3337029646861	8.10620103896224	12.0534787419467	8.31068447380543
12.431475611397	8.25344942505972	12.1603718447009	8.44704962031648
12.5238707656483	8.39477639342094	12.2607803639454	8.57869666600838
12.6109086854524	8.53006975980977	12.3548851278028	8.70534420242559
12.6926085327307	8.659230758308	12.4428877124357	8.82672212038267
12.7689862776801	8.78217386524465	12.5250091607336	8.94257147528718
12.8400575751293	8.89882343220819	12.6014836576652	9.05264744090677
12.9058374676578	9.00911273649504	12.6725553381109	9.15671975694859
12.966339783806	9.11298337952578	12.7384753897862	9.25457275413289
13.0215763666526	9.21038493081124	12.7994993469949	9.34600507371819
13.0715562358816	9.30127474695562	12.8558845029079	9.43082916669284
13.1162848659257	9.38561785547954	12.9078872881348	9.50887069754809
13.1557635363058	9.46338693573356	12.9557606890839	9.57996783489277
13.1899886981975	9.53456242799682	12.9997517907035	9.64397041201692
13.2189515441914	9.59913265653896	13.0400992840101	9.7007390853431
13.2426369389861	9.65709443757105	13.0770318065491	9.75014403292228
13.2610132601093	9.70845883427253	13.110775590857	9.79205854309205
13.2740438640584	9.75324480944788	13.1415407277697	9.82636475413771
13.2816959027117	9.79147480504147	13.169510339828	9.85295752608832
13.2838922200725	9.82320155459028	13.1948869525199	9.87171714778317
13.2805772298468	9.84847231225713	13.2178251781941	9.88254470353655
13.2716598286538	9.86736069755147	13.2384876705816	9.88532990693529
13.2570288524112		9.87995878137326	

6.2 First Stage Rotor Airfoil Coordinates

X Lower Profile	Y Lower Profile	X Upper Profile	Y Upper Profile
0.00260541367538722		8.58102217439199	
0.0118783373181792	8.56283473110548	0	8.60127733100773
0.0280477046339554	8.54568430112805	0.00384038842356526	8.62460302710053
0.0510164144329124	8.5295650430023	0.0142452086131545	8.65092166355734
0.0806976275530789	8.51441137349961	0.0313366852420961	8.68016035823469
0.116993250923096	8.50017335668537	0.0552614162243509	8.71217645591987
0.1598154249634	8.48675035686207	0.0861678629257323	8.74682512537598
0.209077256781204	8.4740261430633	0.124214320176647	8.78392584722871
0.264694508269029	8.4618683229902	0.169565670028573	8.82326490389904
0.326587325174519	8.45012726481359	0.222389848888899	8.86459870000317
0.394680846839613	8.43863876032584	0.282855206542107	8.90765364442893
0.468905684955838	8.42722719526088	0.351127789250413	8.95212581093029
0.549198555571431	8.41570805381085	0.42736828538006	8.99768153097017
0.635502988210225	8.40388973674639	0.511728734305336	9.04395891840844
0.727769973419767	8.39157491492155	0.604349163584854	9.09057008166336
0.825958440104442	8.37856157472864	0.705354290820197	9.13710384276665
0.930035154257121	8.3646461940135	0.814850727543271	9.1831264995456
1.03997388238367	8.34963248511091	0.932924871720418	9.22817716796463
1.1557571606994	8.33332063734618	1.05963817831893	9.27178274511912
1.27737540114578	8.31550890069303	1.19502510776808	9.31346062337986
1.40482580644576	8.29599420932407	1.33909131104186	9.35272242869659
1.5381101191364	8.27459276944138	1.49181305714456	9.38905783018505
1.67723535883333	8.25112267189884	1.65313377894798	9.42195633197353
1.8222120805113	8.22539224382791	1.82296323399861	9.45092330477019
1.9730512626154	8.19720826162864	2.00117819980219	9.47547610685373
2.12976317721183	8.16641199881564	2.18762137834988	9.49511229365405
2.29235599729568	8.13284265728202	2.38210078013551	9.50935034080493
2.46083128251814	8.09632106250651	2.58439246991896	9.51774997456345
2.6351810674547	8.05666885344559	2.79424197155659	9.51989685442858
2.81539265171756	8.01376802154328	3.01135825175472	9.51534673042256
3.00143891562264	7.96747433621938	3.23542247572523	9.50371551604829
3.1932734956499	7.91762356677364	3.46609221455939	9.4846763469803
3.39083188455482	7.86406344724348	3.70300005074159	9.45793066069682
3.5940464060424	7.80672972165598	3.94573864028008	9.42313494322027
3.8028172134939	7.74549648706298	4.19389008737273	9.38005291114775
4.01701305977447	7.68021470605109	4.44702588694568	9.3285192448918
4.23648210053804	7.61076777463866	4.70469717193733	9.26838597693926
4.46108179246767	7.53716556029958	4.96640620009547	9.19943011226118
4.6906160273203	7.4593155911841	5.23167093256303	9.12158379385906
4.92484635380938	7.3770922508456	5.50001584235211	9.03486615538772
5.16356646715374	7.29055279098974	5.77089976007706	8.93916804677461
5.40639791676087	7.19936635074665	6.04392279084843	8.83482344493396
5.65311372339773	7.1037046516791	6.31850559264516	8.72171888308385
5.90347156790799	7.00373403908438	6.59405933323391	8.59980123289366
6.15703488868852	6.899224219145	6.8701679651852	8.46946849668193
6.41342702253398	6.79017304974692	7.1463376589768	8.33094426052302
6.6722838232157	6.67666252533688	7.42204793247468	8.18442067836591
6.93320193953158	6.55874176952155	7.69680726600741	8.0301741856204
7.19574508816576	6.43644505927472	7.97015083720036	7.86854593205555
7.4594472081447	6.30979994673234	8.24164145710752	7.6999318831572
7.72385692489033	6.17890406071657	8.51082924706675	7.52470402419618
7.98850647195736	6.04386047066256	8.77728687500671	7.34327280183626
8.25291433135595	5.90478005276088	9.04061105680483	7.1560823819184
8.51657676574295	5.76176623200765	9.30043511589745	6.96362336895719
8.77899816929379	5.614960258521	9.55640264109715	6.76638484882545
9.03968653299473	5.46452754301196	9.80817591422588	6.56486525000631
9.29814976727168	5.31064765817439	10.0554433328691	6.35957943717412
9.55389770126042	5.15351376103659	10.297920978328	6.15105630267266
9.80644050971909	4.99332744848199	10.5353575485848	5.93984086420948
10.0553103037024	4.83032369280769	10.7675158926794	5.72646624217159

X Lower Profile (Cont)	Y Lower Profile(Cont)	X Upper Profile(Cont)	Y Upper Profile(Cont)
10.3000547098465	4.66475705914577	10.9941822961102	5.51146433459939
10.5402387912813	4.49690012050142	11.2151671408883	5.29536429335969
10.7754470421697	4.32704216975034	11.4303051872804	5.07869072075765
11.0052828820405	4.15548530790859	11.6394580326963	4.86196452500831
11.2293836633718	3.98255792959439	11.8425007186365	4.6456864304068
11.4474170088828	3.80860622077036	12.0393266565158	4.43034254277888
11.6590820516109	3.63399195005717	12.229847289573	4.2164037033997
11.8641111573742	3.45909100061248	12.4139909046648	4.00432419758622
12.0622682294211	3.2842887470115	12.5917044907131	3.79454372537246
12.2533570547799	3.10998550342978	12.7629451840701	3.5874794183966
12.4372204374258	2.93659259475457	12.9276805586823	3.38352736034366
12.6137383779165	2.7645280938573	13.0858895075923	3.18306457518915
12.7828276990408	2.5942143899603	13.2375613255711	2.98644932428124
12.9444411231712	2.42607560892936	13.3826949995942	2.7940216958927
13.0985676311498	2.26053643056711	13.5212968927004	2.60610294513588
13.2452325929714	2.09802087169592	13.6533783491623	2.42299501695441
13.3844936458147	1.9389479365011	13.7789572662911	2.24498335079932
13.5164381878986	1.78372914702548	13.898057787756	2.07233795280931
13.6411809113669	1.63276650279279	14.0107097208627	1.90531418392799
13.7588614302863	1.48645086324021	14.1169476494168	1.74415326646829
13.8696452506963	1.3451629866089	14.216806524764	1.58908027053691
13.9737178329923	1.20926977982589	14.3103240158119	1.44030701981797
14.0712789160637	1.07912134568785	14.3975424809916	1.29803432351913
14.162541217869	0.955051415201614	14.4785064808512	1.16245093893604
14.2477278158807	0.837377003382007	14.5532615619311	1.03373341796601
14.3270695336245	0.726398241023094	14.6218530201861	0.912045876133636
14.40080217863	0.622398262430642	14.6843248332221	0.797539794799301
14.4691636592833	0.525643154162502	14.7407187682422	0.690353841874448
14.5323911962756	0.436382076306309	14.791073483877	0.590613589731721
14.5907188821805	0.354847670384778	14.8354234054286	0.498431006416965
14.6443757139262	0.28125677760784	14.8737972807171	0.413903686752068
14.6935840118694	0.215811370514384	14.9062165333971	0.337113910833178
14.7385578905958	0.158699476009465	14.9326937775264	0.268127742827462
14.7795010024427	0.110095644082234	14.9532322993903	0.206994607171319
14.8166012791039	0.0701597206452149	14.9678288060649	0.153748575706235
14.8500428295016	0.0390450445283559	14.9764593049988	0.10840023838608
14.8799977535222	0.0168952869907137	14.9790853749109	0.0709399326423501
14.9066165908684	0.00384066300349239	14.9756621258914	0.0413415964675163
14.9300296218175	0	14.9661356461529	0.0195607547693903
14.9503944832629		0.00550764966568629	

6.3 Second Stage Stator Airfoil Coordinates

X Lower Profil	Y Lower Profil	X Upper Profil	Y Upper Profil
0.00254196655982694		1.08115141252134	
0	1.05948129331135	0.0126751465815545	1.10046566470334
0.00480944090706062	1.03438957742082	0.0306480439010552	1.11851968595974
0.017084217203501	1.00592989170702	0.056372650883324	1.13534937648128
0.0369640033220907	0.974220645375984	0.0897519178547126	1.15098489911519
0.0645874435786821	0.939362966408981	0.130705672190229	1.16553178797877
0.100116519152637	0.901528196357853	0.179145062799617	1.17908212584386
0.143717730888661	0.860902987363826	0.234989869686534	1.19176775547833
0.195565063955998	0.817707239855099	0.29816372763888	1.20374029799322
0.255837318175853	0.772194095419161	0.368594698399012	1.2151687775804
0.32471502437263	0.724648921387132	0.446215992014215	1.22623793225442
0.402377265294019	0.675388207474348	0.530966542578621	1.23714630855289
0.488998468145753	0.624758502459584	0.622791397555872	1.24810403252008
0.584745853066365	0.573138713522844	0.721641264826589	1.2593269565152
0.689775562356298	0.52093695065364	0.827473223084457	1.27103602328153
0.80422868416888	0.468585606935344	0.940251413996081	1.28345818182568
0.928227886303372	0.416537730074492	1.05994703399174	1.29682582640853
1.06187534822743	0.36527072578844	1.1865369721383	1.31136874582071
1.20525018333112	0.315289569274626	1.32000293741847	1.32730643541339
1.35840296479039	0.267104200105795	1.46033349778173	1.34486612592835
1.52135441863492	0.221229261756134	1.60752200319672	1.36427839778708
1.69409507492484	0.178200648253568	1.7615636373706	1.38575594846454
1.8765820451084	0.138568219673872	1.92245546504362	1.40949618138821
2.06873604246102	0.10285770484644	2.09019639201961	1.43571462796445
2.27044268482466	0.0715855901056319	2.26478303153371	1.46462543346928
2.48155118630956	0.0453051317495778	2.44620840156344	1.49639079809955
2.70187286563291	0.0245282775814117	2.63446105482808	1.53119461594889
2.93118385765258	0.0097275412218758	2.82952028220796	1.56923629534264
3.16922323691074	0.00138775132223601	3.03135620566772	1.6106748643214
3.41569079997478	0	3.23993053616402	1.65563106148827
3.67025682689747	0.00596591639261224	3.45518569563634	1.70427930931613
3.93256099670599	0.0196548948581952	3.67704514455438	1.75678696168024
4.20219730254591	0.0415022971806096	3.90542808257807	1.81321282572055
4.47873878778006	0.0718313127007189	4.14022471087807	1.87368229161955
4.76174080653119	0.110882282670335	4.38129335903725	1.93835527944979
5.05071696493976	0.158945522279104	4.62848532316057	2.00729098294761
5.34514610708712	0.216304254934645	4.88163905059104	2.08050280672742
5.64451271284064	0.283079146923815	5.14054129976402	2.15811201764066
5.94830269017724	0.359292277849758	5.40493328489784	2.24028228142305
6.2559171749852	0.445171467058967	5.67459918129805	2.32691416864687
6.56667378579617	0.541077762139316	5.94936752921126	2.41771682582699
6.88025848791522	0.646167061188715	6.22866236388027	2.51354583963333
7.19580459468177	0.761208325772987	6.51242752306742	2.61358483470772
7.51294962469997	0.885447388390131	6.80007338926759	2.71848179650846
7.83090293995476	1.01925590848006	7.09141311501945	2.82770055828378
8.14911683957989	1.16230134105383	7.38599562736975	2.94135157923202
8.46704241993615	1.31424530813156	7.68335406940471	3.05949461288994
8.78409766748626	1.47481116043532	7.98304217895931	3.18207246575269
9.09968872362196	1.64372662594223	8.284617630267	3.30896993532249
9.41325183615088	1.82063986894821	8.58760478738854	3.44009958823574
9.72426994891853	2.00510317277098	8.89148288044368	3.57542014829149
10.0322338828978	2.19666148825114	9.19572961309687	3.71485023399009
10.3366388442461	2.39486060320217	9.49982942720573	3.85826267118361
10.6370117399916	2.59920198484391	9.80325090534809	4.00553230871792
10.9329174481508	2.80914156796933	10.1054451261178	4.15654004357103
11.2239602919429	3.02409685151458	10.4058486848725	4.31116867159502
11.5097563192144	3.24349752509569	10.7039157421657	4.46925532078011
11.7899556986989	3.46675296574771	10.9990997529032	4.63062710517278
12.0642434368365	3.69325699774643	11.2908566388161	4.7950995850001

X Lower Profil (cont)	Y Lower Profil (cont)	X Upper Profil (cont)	Y Upper Profil (cont)
12.3323475966033	3.92238174307224	11.5786401910531	4.962486184112
12.5940273071249	4.15349993133874	11.8619173846126	5.13257917499769
12.8490666021403	4.3859958980286	12.1401775395413	5.30514198218186
13.0972824090629	4.61925694478591	12.4129269828916	5.47992111062185
13.3385227677815	4.8526781919019	12.6796931110035	5.65664455020493
13.5726685276854	5.08566252596242	12.9400245854996	5.83502503561174
13.7996308157991	5.31762542780437	13.1934953553077	6.01475835975103
14.0193377983619	5.54801091276356	13.4397189710467	6.19551049336246
14.2317397509592	5.77628480412248	13.6783441689126	6.37692727577733
14.4368065011903	6.00193696348075	13.9090576559738	6.55863504041279
14.6345246682444	6.22448316286232	14.1315866720871	6.74024147894702
14.8248975647704	6.44346376521248	14.3456984663361	6.9213395677975
15.007941224899	6.65844612591953	14.551203231095	7.10150763608869
15.1836752368678	6.86903125901607	14.7479618258481	7.28030502484087
15.3521252678745	7.07484842778208	14.9358814172563	7.45727967261062
15.5133210741719	7.27555432937383	15.1149152599773	7.63197095446721
15.667294751474	7.47083194579803	15.2850618839541	7.80391270001834
15.8140793195419	7.6603890633744	15.4463636181634	7.97263638785992
15.9537077101176	7.84395649292765	15.5989044083846	8.13767448515286
16.0862105138532	8.0212874087804	15.7428086027084	8.29856251655779
16.2116134005016	8.19215694115872	15.8782398222617	8.4548407314932
16.3299386703601	8.35635859637511	16.0053954929977	8.60605880011248
16.4412051692759	8.51370240208614	16.1245028418838	8.75177864654137
16.545428122054	8.66401341259353	16.2358148397714	8.89157679121228
16.6426188760574	8.80713056912353	16.3396061374425	9.02504621501196
16.7327844523181	8.94290597421758	16.4361691366118	9.15179769447982
16.8159269964422	9.07120449185774	16.5258101431773	9.27146070539147
16.8920433583637	9.19190350308622	16.6088454133556	9.38368407437718
16.9611248431813	9.30489279219757	16.6855970899296	9.48813641322018
17.0231568697192	9.41007473526413	16.756389330852	9.58450617397252
17.0781183151621	9.50736490656638	16.8215448898052	9.67250121925239
17.1259806841105	9.59669297331682	16.8813820470646	9.75184804717104
17.1667075849298	9.67800354887941	16.9362114428928	9.82229101029344
17.2002553365947	9.75125649602859	16.9863320234623	9.88359204633561
17.2265742974158	9.81642695921882	17.0320265389225	9.93553065039564
17.2455829491435	9.87352207794959	17.0735845886461	9.97788714480742
17.2572068219229	9.92255800794648	17.1112611539835	10.0104656273718
17.261357866579	9.96357382325674	17.1452950348934	10.0330800315479
17.2579235453866	9.99663912261943	17.1759179389833	10.0455464810471
17.2467732133343	10.0218513398066	17.2033466673009	10.0476859439821
17.2277700998174		10.0393299741723	

6.4 Second Stage Rotor Airfoil Coordinates

X Lower Profil	Y Lower Profil	X Upper Profil	Y Upper Profil
0		12.7545479553707	
0.00826981040518423	12.7284712031389	0.000578037918462396	12.7819072353794
0.0254813123017246	12.7022776545236	0.00992071240504021	12.8119141495354
0.0515206857682209	12.675983877714	0.0281735319794455	12.844449716331
0.0862824110329074	12.6495338685317	0.0554941473279175	12.879400049518
0.129658627709331	12.6228888153556	0.0920619740812301	12.9165677847975
0.181551175318382	12.5959536697085	0.138064741319003	12.9557471654524
0.241868582492156	12.5686108651613	0.193699712453636	12.9966924323456
0.310527295610288	12.5407243268702	0.259170305581016	13.0391163607995
0.387453454172668	12.5121378102607	0.334681827455324	13.0826948875492
0.47258394485199	12.4826774502755	0.420437614029527	13.1270679250812
0.565867217012865	12.4521549791152	0.516635122852382	13.1718398813446
0.667263967625845	12.4203701971471	0.623461900402371	13.216581273454
0.776747606576815	12.387112665347	0.74109154700973	13.260831437904
0.894304390760767	12.3521628938244	0.869679826958488	13.3041020314457
1.01993314005518	12.3152936870697	1.00936104864847	13.3458806287511
1.15364459098505	12.2762811467858	1.16024469862054	13.3856248810928
1.29546092929341	12.234899387514	1.32241182911733	13.4227731445116
1.44541433216775	12.190916152685	1.49591241020354	13.456754352407
1.6035448749582	12.1440944825263	1.68076333388329	13.4869919428476
1.76989878315146	12.0942034924361	1.87694613182594	13.5128987431923
1.94452798160868	12.0410354265945	2.08440349677395	13.5338656082079
2.12748458978688	11.984364190267	2.30304100030477	13.5493085692517
2.31881777926738	11.9239596499854	2.53272663093714	13.558660166714
2.51857292256734	11.859608832413	2.7732882624607	13.5613537969444
2.72679323197666	11.7911390321477	3.02450889077656	13.5568060263768
2.9435055907778	11.7183433875673	3.286137971745	13.5444962779247
3.1687195074209	11.6410115113236	3.55788996181432	13.5239412686987
3.40243472244132	11.5589832390914	3.83943456117371	13.4946461028167
3.64463676275748	11.4721279361395	4.1303993912225	13.4561295490863
3.89527585256744	11.3802694500032	4.43038972021241	13.4080033867944
4.15427154285031	11.2832318755283	4.73898289455105	13.3499306272365
4.42154156535416	11.1809476499021	5.05569898560611	13.2815210698126
4.6969659461107	11.0733249099958	5.38003662875933	13.2024672395264
4.98037518259841	10.9602294172509	5.71148525832295	13.1125653826478
5.27156043318732	10.8415327330787	6.04951579327922	13.01166982251
5.57033657153668	10.7172852542854	6.39351892057684	12.8995220538992
5.87645003304996	10.5874474123569	6.74289904408523	12.7760212632525
6.18958265631799	10.451924452308	7.09707268731103	12.6411908531261
6.50932229063751	10.3105145308614	7.45550056571995	12.4952312284549
6.83566547441851	10.1640468616773	7.81718800678041	12.3373821172639
7.16762028577389	10.0112091487032	8.18208559550558	12.1690951881945
7.50522464927812	9.8530852707383	8.54907473689298	11.9894960081663
7.84792519764552	9.68952222687776	8.91759300842336	11.7990163398026
8.19511003638324	9.52036152032384	9.28710592324338	11.5981616131974
8.54632625923556	9.34583946952994	9.65689422193546	11.387109097744
8.90103545620012	9.16608676305588	10.0263034141526	11.1662064747998
9.25864984867493	8.98120605038806	10.3947128962808	10.9358920383729
9.61852966219207	8.79127013584691	10.7615439934029	10.6966939782364
9.98006998704494	8.59646485996866	11.1261786323616	10.4490846844912
10.342640759079	8.39697600428794	11.488024969506	10.1935907627114
10.7055893417795	8.1929906624974	11.8465204469925	9.93078834317772
11.0682263807726	7.98467342321805	12.2011515610687	9.66132336661845
11.4298759543941	7.7722388891407	12.5514092731867	9.38583535027692
11.7898660247935	7.55592876019881	12.896804014333	9.1049764358897
12.1475207915656	7.33599496171457	13.2368786362021	8.81942426829111
12.502162172702	7.11269742182093	13.5712120411984	8.52988013015059
12.8531094214471	6.88629976151138	13.8994244410094	8.23706909919977

X Lower Profil (cont)	Y Lower Profil (cont)	X Upper Profil (cont)	Y Upper Profil (cont)
13.1997110322571	6.65710627169153	14.2211500508005	7.94169888293264
13.5413320580496	6.42543864082691	14.5360540593762	7.64447889594783
13.8773572547696	6.19163499030421	14.8438334244319	7.34611705075218
14.2071920902895	5.95604657215846	15.1442194239678	7.04731893425866
14.5302655477634	5.71903701324169	15.4369780050568	6.7487845115299
14.846050090925	5.48100072132839	15.7218925372761	6.45118576544412
15.1540545919226	5.24234941779551	15.9987731487257	6.1551763301854
15.4538271080691	5.00351094108509	16.2674557406872	5.86138899509742
15.7449567094255	4.76492724574287	16.5278014655103	5.57043417291981
16.0270720806233	4.52704944805112	16.7796989350338	5.28290149814746
16.2998558787157	4.29034902855253	17.0230501727497	4.99934545981934
16.5630402952425	4.05530947750537	17.2577748608743	4.72029079506742
16.8164064894273	3.82242268566526	17.4838102191002	4.44623335111428
17.0597847137868	3.59218646600203	17.7011097017759	4.17764003787331
17.2930529845146	3.36510113345811	17.9096426734337	3.91494994947731
17.5161394309843	3.14166978629556	18.1093899447605	3.65857201430276
17.7290226174819	2.92239686779201	18.3003408963549	3.40888459556014
17.9317263731878	2.70778240223679	18.4824956785421	3.16623964710339
18.1243172082396	2.49831917376187	18.6558644373279	2.93096415237881
18.3069014642443	2.29449016967575	18.8204664494203	2.70336151924805
18.4796233703182	2.09676718848031	18.976328029638	2.48371202297238
18.6426661566848	1.90561210697547	19.1234770958774	2.27227079361838
18.7962419006639	1.72146974603239	19.2619487564788	2.06927439731718
18.940588299397	1.54476686124869	19.391783767443	1.87494147268823
19.0759653040554	1.37591135708313	19.5130269683007	1.68947331004375
19.2026516220495	1.21529170859999	19.6257257350331	1.51305437433341
19.3209412549254	1.06327668486005	19.7299283282393	1.34585266195553
19.431139811094	0.920215159490485	19.8256824438522	1.18802008934229
19.533560492492	0.786435926016186	19.913034113895	1.03969297866103
19.6285199663344	0.66224764440873	19.9920267924477	0.900992496796402
19.7163345379219	0.547939153539083	20.0627002565089	0.772024795455408
19.797316977357	0.443780310095674	20.1250890134667	0.6528806744794
19.8717740898362	0.350023330661138	20.1792201685969	0.543634774639301
19.9400048142323	0.266904431659764	20.2251110090958	0.444344488695759
20.002298345254	0.194645410392313	20.2627668483544	0.355048931718281
20.0589312910772	0.133454549087258	20.2921801549894	0.275768573845234
20.1101610813503	0.0835251729330846	20.3133337852415	0.206507190702835
20.1562270203287	0.0450387825854346	20.326196954294	0.147249198402333
20.1973765395136	0.0181829902120665	20.330696418974	0.0979421328392061
20.2338036453373	0.00311654288901586	20.3267758994209	0.0585319797694606
20.2656967244696	0	20.3143465963584	0.0289327809110098
20.2932622629173		0.009011287156234	

6.5 Third Stage Stator Airfoil Coordinates

X Lower Profil	Y Lower Profil	X Upper Profil	Y Upper Profil
0		0.964516879090533	
0.00100237474451441	0.933882640066281	0.00963035208265782	0.993605161178072
0.0125339044919618	0.900175293244523	0.0300096617190022	1.02271229229817
0.0347413007192474	0.863481896679919	0.061028947901651	1.05186391746446
0.0677996418511487	0.823986491501461	0.102575197981224	1.0810629616874
0.111891094621796	0.781837950793219	0.154551427348608	1.11042047920659
0.167220284211104	0.737283393062955	0.216859619786765	1.14002043047625
0.233999773797045	0.69058754494745	0.289413104688317	1.1699980152265
0.312449708613588	0.642056254434757	0.372134337427096	1.20051337682132
0.402793983512571	0.592036776050556	0.464955749605876	1.23174807636671
0.505255998108763	0.540915764743454	0.56782063492461	1.2639034229771
0.620054358916328	0.489117089044846	0.68068374491031	1.29719857582774
0.747398652846384	0.437100378453489	0.803511507300848	1.33186753209997
0.887485450867453	0.385363995017365	0.936281748609608	1.36815134252975
1.04049362992026	0.334438306118105	1.07898387589927	1.40629971161457
1.20658016153685	0.284879357237302	1.23161841482368	1.44657191987047
1.38587640861659	0.237263691168697	1.39419590995902	1.48923635967517
1.57848473063719	0.192198835972605	1.5667354361416	1.53455420193349
1.78447450821082	0.150315883384933	1.7492636599616	1.58278081261172
2.00387942681293	0.112246067281563	1.94181266224042	1.63418305120976
2.23669567789158	0.078620378593136	2.14441691406087	1.68903345703605
2.48287766142094	0.0501033855665598	2.35711287270898	1.74757019691482
2.74233679781165	0.027354517268493	2.57993563920927	1.81002955889788
3.01494291208782	0.0110008875434285	2.81291326284425	1.87666695685521
3.30052191353748	0.0016615873211151	3.0560650160015	1.94772655943869
3.59884688325149	0	3.30940657129463	2.02338302907378
3.90965103562132	0.00660497935081139	3.57293365663824	2.10385457060928
4.23262703044268	0.0220181198348107	3.84661975037389	2.18937009721083
4.56741039815079	0.0468272720117648	4.13043008928724	2.2800703964364 1
4.91359223320461	0.0815761662538411	4.4243068661481	2.3760934667695
5.27073387683489	0.126706389681064	4.72815292318431	2.477627810828
5.63835162785714	0.182644447455905	5.04184592612037	2.58482098267184
6.01589324807523	0.249885081986538	5.36526127106308	2.69769224145442
6.40279755994675	0.328750455682436	5.69821244065667	2.81636972863462
6.79848150934814	0.419474507583359	6.0404644459015	2.94100287821063
7.20227589163491	0.522421014950358	6.39179915970868	3.07154154547501
7.61349605688606	0.637831692345133	6.75194622554733	3.20798553506813
8.03147070577828	0.765767745672548	7.12055642395009	3.35044112081213
8.45550673617996	0.906240934264386	7.49723952599877	3.49898851082403
8.88477670192638	1.0595101147736	7.88168005661974	3.65338428732881
9.31839518566611	1.22583516552907	8.27356464529491	3.81330692234836
9.75595258830743	1.40420474175606	8.67205243652832	3.97962891537199
10.1962595203462	1.59544785861721	9.07703534524045	4.15130554932621
10.6388905435259	1.79849334287668	9.48759937492892	4.32911621417756
11.0826710300351	2.0139170241117	9.9035431938071	4.51211841437178
11.5269280813146	2.24109566465143	10.324132985716	4.70049544519894
11.9709424094578	2.47949149303683	10.7486566285074	4.89427385487525
12.4138827375681	2.72876387580809	11.1764955964132	5.09321413662701
12.8549452533557	2.98848083138324	11.6069920026144	5.29710192382559
13.293368581543	3.25810754479127	12.0394402649875	5.5057625041695
13.7284619048769	3.53697478232904	12.4730657122831	5.71909572679473
14.1595056592541	3.82446858273677	12.9071306512649	5.93688989711325
14.5858058593975	4.11993622248614	13.3408867838607	6.15891963188976
15.0067097272267	4.42267001087702	13.7735662476168	6.38496608794491
15.4216277672923	4.73188433043372	14.2043660809534	6.61484411733525

X Lower Profil (cont)	Y Lower Profil (cont)	X Upper Profil (cont)	Y Upper Profil (cont)
15.8299951435242	5.04678833410966	14.6324932057545	6.84833390537743
16.2312721247077	5.36659033210223	15.057170108055	7.08518102640491
16.6249654086477	5.6904720394027	15.4776193569018	7.32512671391181
17.0106299360589	6.01759419791656	15.8930673026971	7.56790679938775
17.387881084289	6.34708764316349	16.3027370200013	7.8132652185969
17.7563608818953	6.67810656863971	16.7058868120056	8.06090530185708
18.1157526275059	7.0098118745457	17.1017998549951	8.31051093237177
18.4657835528764	7.3413719629353	17.4897853085159	8.5617501826605
18.8062233361178	7.67196850494636	17.8691830550768	8.81427387708393
19.1368918668005	8.00079034211015	18.239358641947	9.06772589387358
19.4576371389193	8.32706284587884	18.5997275280285	9.32171785985782
19.7683369361552	8.65004597634006	18.9497549552203	9.57583497632317
20.0689000665277	8.96903282503062	19.2889556760758	9.8296411727174
20.3592628516923	9.28335316021668	19.6168978265434	10.0826790537627
20.6393865421466	9.59237514935501	19.9332052717786	10.3344714516044
20.9092596432475	9.89550141234522	20.2375544446003	10.5845284181896
21.1688803599256	10.192185132323	20.5296904783681	10.832333922431
21.4182582001168	10.4819247544515	20.8094236090352	11.0773537155178
21.6574128786858	10.7642615089992	21.0766277243603	11.3190401244043
21.8863715412639	11.0387783875796	21.3312400654285	11.5568351433869
22.105166392315	11.3050984641576	21.5732600253424	11.7901739333496
22.3138328211665	11.5628826057061	21.8027469848679	12.0184886873101
22.5124079897451	11.8118267376842	22.0198172588675	12.2412127028203
22.700924252073	12.0516635830496	22.224645824767	12.4577797503339
22.8794104847398	12.28215734929	22.4174597984932	12.6676302728285
23.0478922789865	12.503099853745	22.5985327548723	12.8702159379744
23.206391366073	12.7143076565611	22.7681795709832	13.0650029866834
23.3549250892235	12.9156194914338	22.9267510314402	13.2514751024853
23.4935057336793	13.1068941646163	23.074628437982	13.4291356470714
23.6221396612209	13.2880089622096	23.2122183320707	13.597509238824
23.7408264707987	13.4588583925047	23.3399471645999	13.7561428651824
23.8495584784949	13.6193530581089	23.4582556754037	13.9046067523036
23.9483204143587	13.7694187565781	23.5675931406176	14.0424949118257
24.0370888496512	13.9089961562759	23.6684120291375	14.1694250366516
24.1158310929157	14.0380411870069	23.7611633832368	14.2850376247378
24.1845038688743	14.156525871336	23.8462926610445	14.3889946231632
24.2430525165489	14.2644390649844	23.92423535395	14.4809781417283
24.2914118342925	14.3617863566878	23.995411298035	14.5606900025782
24.3295099883273	14.4485882266695	24.060216306629	14.6278530426186
24.3572338504961	14.5249040071997	24.1190527984918	14.6821866400339
24.3744686436109	14.5908062920411	24.1722865796053	14.7234318315728
24.3810970573005	14.6463831635615	24.220244647876	14.7513486638236
24.3769542499346	14.6917690302166	24.26325763292	14.7656849961659
24.3618572143065	14.7271267481341	24.3016284162968	14.7661940903434
24.3356177287059		14.7526410101499	

6.6 Third Stage Rotor Airfoil Coordinates

X Lower Profil	Y Lower Profil	X Upper Profil	Y Upper Profil
0		20.0062170707748	
0.00642656511108529	19.9675011939282	0.0060924042295503	20.0449984048646
0.0252437989722335	19.9268684551111	0.0248490979350174	20.0857816824259
0.0563193390332751	19.8843631096787	0.0564531964201783	20.1283854941038
0.0995284086572592	19.8399470598234	0.101113047648089	20.172620494975
0.154756315259924	19.7935808491934	0.15905821969744	20.2182101217951
0.221900941354892	19.7451719362495	0.230534910432931	20.2648446982588
0.300874738182649	19.6945874316477	0.315801290361336	20.3121717251651
0.391606776157446	19.6416695131398	0.415122250659657	20.3597841193312
0.494044347297494	19.5862334002363	0.528764092759187	20.4072264916889
0.608154188625142	19.5280697306201	0.656989127084571	20.4539975908184
0.73392330156683	19.466947901693	0.800050247201939	20.4995523125947
0.871359266962933	19.4026187058801	0.958185625365825	20.5433049074942
1.02048996044811	19.3348161932919	1.13161367419786	20.5846334085661
1.18136261104698	19.2632591377701	1.32052838458121	20.6228848574242
1.35404324413354	19.1876615226432	1.52509405449578	20.6573718624787
1.53861524676437	19.1077353958489	1.74544072908433	20.6873770878447
1.73517572143166	19.0231817158368	1.98166174608891	20.7121699975818
1.94383213166824	18.9336925363163	2.23381094473792	20.7310124516698
2.16469919435728	18.8389574487525	2.5018996454983	20.7431601781263
2.3979014428286	18.7386995047301	2.78588803905412	20.747834841755
2.64356082562454	18.632625527814	3.08569168166575	20.7442817422526
2.90179202441879	18.5204339591502	3.40118047447911	20.7317699399845
3.17270044229585	18.401832336699	3.73217523507602	20.7095826527508
3.45639239755063	18.2765963442824	4.07843238349328	20.6769659316681
3.75294678825785	18.1444683850859	4.43966753219929	20.633237607361
4.06241378475386	18.0051837116854	4.81555247446051	20.5777684221706
4.38482344964772	17.8585203206632	5.20570271940624	20.5099390904421
4.72019665515686	17.7043402878039	5.60966324781922	20.4291055637392
5.06849523166914	17.5424415588359	6.02695559405335	20.3347534419356
5.4296336519863	17.3726216662832	6.45706398403246	20.2264400189292
5.80351975744944	17.1948007514463	6.89939305231169	20.1036765469595
6.19002025180908	17.0089212284884	7.35330143601122	19.9660333495055
6.58892071628571	16.8148577768315	7.81814151010394	19.8132340676906
6.99994775480869	16.6124929576976	8.29323766707047	19.6450837198603
7.42286088277037	16.4019322178904	8.77779553353078	19.4612567912588
7.85732579306161	16.1831958133386	9.27103048990482	19.2616078059441
8.30291142411042	15.9562337418246	9.77217306205285	19.0461582808835
8.75910803798953	15.7209791136696	10.2804539643959	18.8150446275731
9.22551328576463	15.4777208803559	10.7949217988976	18.5681460800485
9.70190807745099	15.2271965153538	11.3143715682282	18.3049920585618
10.1868247715907	14.9678752814834	11.8387814581286	18.0274783427444
10.680484781974	14.7015695240896	12.3663807560698	17.7342546276063
11.1816432907074	14.4274492883393	12.8968111765268	17.4267081810214
11.6898585397744	14.1462604725348	13.4288640754852	17.1047434118883
12.2043029704772	13.8581453278035	13.961676235204	16.7689585635887
12.7241218280234	13.5632959302559	14.4943785484554	16.4199889352796
13.2483961222658	13.2618861600016	15.0261406542691	16.0585711286029
13.7762798118573	12.9542804444403	15.5560415980042	15.6853300974157
14.3068703258438	12.6408125334736	16.0832073393931	15.3009957706128
14.8392194251288	12.3218001074661	16.6068080419242	14.9063834872786
15.3723160709433	11.9975170205998	17.1260834109373	14.5024164835678
15.9051880759113	11.668334853689	17.6402492386369	14.089978800872

X Lower Profil (cont)	Y Lower Profil (cont)	X Upper Profil (cont)	Y Upper Profil (cont)
16.4368535753522	11.3346403705841	18.1485540520548	13.6699920659731
16.9663186396214	10.9968251003254	18.6502894773107	13.2434199666337
17.4925687621427	10.6552681447992	19.1448065207215	12.8112793688855
18.014597375212	10.3103684305486	19.6314945515342	12.3746019033579
18.5314325580607	9.96257061676042	20.1097617608501	11.9344018542161
19.0421169813146	9.612330518605	20.5790619944193	11.4917045363316
19.5457152183882	9.26011758439866	21.0388937738627	11.0475376658376
20.0413061673169	8.90639970106459	21.4888137116849	10.6029404916921
20.5280149269812	8.55167528296634	21.9284099292295	10.1589257733963
21.0050169561936	8.19647043305726	22.3573026068692	9.7164768539531
21.4715336481753	7.84132707412995	22.7751524967089	9.27655396582229
21.9268377787287	7.4868032727797	23.1816589076792	8.84008858003599
22.3702501003604	7.13346431837484	23.5765658646189	8.40798726595914
22.8011551906279	6.78189496610555	23.9596483128344	7.98111467918899
23.219009902483	6.43270288679201	24.3307050062171	7.5602856580894
23.6233376192892	6.08650772141654	24.6895648683229	7.14627205063796
24.0137302646887	5.74393911003412	25.0360848746199	6.7398009179326
24.3898483693396	5.4056332556845	25.3701491585877	6.34155456602007
24.7514199725306	5.07222896614165	25.6916685746487	5.95217147174312
25.0982514251426	4.74437525505713	26.0005676686412	5.57223602582942
25.4302197766677	4.42272167636448	26.2967893963427	5.20228592041538
25.7472696542777	4.10791391059021	26.580294711112	4.84281465977079
26.0494104764479	3.80059035800607	26.8510612127811	4.4942734331567
26.3367134393232	3.50137916011878	27.1090814595315	4.15707291877979
26.6093127050628	3.21089931131785	27.3543565583542	3.83158134424392
26.8673989320211	2.92975566153634	27.5868969436028	3.51812898682454
27.1112118739081	2.65853400838418	27.806723669945	3.2170128964729
27.3410355372117	2.39779904702879	28.0138667874928	2.92849905207833
27.5571931786628	2.14809274139133	28.2083635774927	2.65282436393321
27.7600425107986	1.90993335936191	28.3902563432491	2.39019825421383
27.9499709319448	1.68381496432482	28.5595900046993	2.14080399601554
28.1273903961155	1.47020702987665	28.7164099473023	1.90480011552634
28.2927327392006	1.26955475329062	28.8607593758789	1.68232125222289
28.4464396067678	1.08227579097419	28.9926820953155	1.47348272359226
28.5889581688077	0.908761643170134	29.112219599687	1.27838053653603
28.7207379413335	0.749379931065945	29.2194072158099	1.09709057170149
28.8422261361986	0.604475680849895	29.3142719442355	0.929668795955394
28.953862998049	0.474372658651152	29.3968306010176	0.776151429497236
29.0560772273252	0.359374770404898	29.4670882209085	0.636555025011127
29.1492871263493	0.259771233363455	29.5250311413025	0.51087272489524
29.2338967620051	0.175838149154032	29.5706255260562	0.399074041044038
29.3102859506867	0.107835882979618	29.6038225719552	0.301108728857979
29.3787949911752	0.0560029638270407	29.6245695159945	0.21691401903928
29.4397923856147	0.0206039659500838	29.6327382421047	0.146367727712683
29.4935594316537	0.00185700074805339	29.6282376377077	0.0893615991491714
29.540387072735	0	29.6109143408964	0.0457356862994303
29.5805634533235		0.0152847743382125	

Note

For every blade, the beginning and final x and y coordinates are the same for the upper and the lower profile (this makes them joined and yields to a complete blade profile) The methodology followed was to concentrate the number of points near the leading and trailing edges to smoothen the curve near these areas (due to the high tangent). For our work, we took 300 points per section (600 in total Upper + Lower).

The given coordinates in this appendix has only 100 points per section (200 in total) which has a less smoother profile near the leading and trailing edge but is enough to perform a numerical simulation to any reader that desires to reproduce the work, or to investigate our blades for all the three stages of the turbine, individually or collectively.